Pyrazolate-based cobalt(II)-containing metal-organic frameworks in heterogeneous catalytic oxidation reactions: elucidating the role of entatic states for biomimetic oxidation processes

Markus Tonigold, Ying Lu, Andreas Mavrandonakis, Angela Puls, Reiner Staudt, Jens Möllmer, Joachim Sauer, Dirk Volkmer

Angaben zur Veröffentlichung / Publication details:

Tonigold, Markus, Ying Lu, Andreas Mavrandonakis, Angela Puls, Reiner Staudt, Jens Möllmer, Joachim Sauer, and Dirk Volkmer. 2011. "Pyrazolate-based cobalt(II)-containing metal-organic frameworks in heterogeneous catalytic oxidation reactions: elucidating the role of entatic states for biomimetic oxidation processes." *Chemistry: A European Journal* 17 (31): 8671–95. https://doi.org/10.1002/chem.201003173.

Pyrazolate-Based Cobalt(II)-Containing Metal–Organic Frameworks in Heterogeneous Catalytic Oxidation Reactions: Elucidating the Role of Entatic States for Biomimetic Oxidation Processes

Markus Tonigold,[a] Ying Lu,[a] Andreas Mavrandonakis,[b] Angela Puls,[c] Reiner Staudt,[d] Jens Möllmer,[e] Joachim Sauer,[b] and Dirk Volkmer*[a]

Abstract: Crystal structures of two metal–organic frameworks (MFU-1 and MFU-2) are presented, both of which contain redox-active Co^{II} centres coordinated by linear 1,4-bis[(3,5-dimethyl)pyrazol-4-yl] ligands. In contrast to many MOFs reported previously, these compounds show excellent stability against hydrolytic decomposition. Catalytic turnover is achieved in oxidation reactions by employing *tert*-butyl hydroperoxide and the solid catalysts are easily recovered from the reaction mixture. Whereas heterogeneous catalysis is unambiguously demonstrated for MFU-1, MFU-2 shows catalytic activity due to slow metal leaching, emphasising the need for a deeper understanding of structure–reactivity relationships in the future design of redox-active metal–organic frameworks. Mechanistic details for oxidation reactions employing *tert*-butyl hydroperoxide are studied by UV/Vis and IR spectroscopy and XRPD measurements. The catalytic process accompanying changes of redox states and structural changes were investigated by means of cobalt K-edge X-ray absorption spectroscopy. To probe the putative binding modes of molecular oxygen, the isosteric heats of adsorption of O_2 were determined and compared with models from DFT calculations. The stabilities of the frameworks in an oxygen atmosphere as a reactive gas were examined by temperature-programmed oxidation (TPO). Solution impregnation of MFU-1 with a co-catalyst (*N*-hydroxyphthalimide) led to NHPI@MFU-1, which oxidised a range of organic substrates under ambient conditions by employing molecular oxygen from air. The catalytic reaction involved a biomimetic reaction cascade based on free radicals. The concept of an entatic state of the cobalt centres is proposed and its relevance for sustained catalytic activity is briefly discussed.

Keywords: cobalt · heterogeneous catalysis · oxygen · thermodynamics · metal–organic frameworks

Introduction

Porous metal–organic frameworks (MOFs) constitute a rapidly emerging class of multifunctional hybrid materials that might be useful for diverse technical applications, such as gas or liquid adsorption and separation, molecular recognition or catalysis.[1,2] By combining bi- or multifunctional ligands (predominantly polycarboxylate ligands) and (transition) metal ions, moderately robust MOFs can be prepared, of which 1,4-benzenedicarboxylate (bdc) represents a versatile linker, for instance, leading to the porous frameworks MOF-5 ($[Zn_4O(bdc)_3]$),[3] and MIL-101 ($[Cr_3O(OH,F,H_2O)_3(bdc)_3]$),[4] which are now regarded as archetypal examples of coordination polymers that exhibit permanent porosity upon solvent removal.

Developing MOFs into heterogeneous catalysts could yield several principal advantages, such as enhanced catalyst stability due to the spatial separation of single catalytic sites in the framework.[5] MOFs can possess high porosities in the absence of any inaccessible bulk volume (dead volume),[2] and most evidently their pore size(s), and thus their substrate shape and size selectivity, can be systematically tailored by employing different organic linkers.[6] MOF prototypes, such as the recently described MFU-4[7a] or magnesium formates,[2,7b–d] possessing narrow and structurally well-defined pores, can be used to separate gas mixtures containing molecules with very similar shapes and kinetic diameters (e.g., separation of H_2 from O_2/N_2).[2,7a,c] On the other hand, the pores in MOF-5, for instance, are sufficiently large to

[a] M. Tonigold, Dr. Y. Lu, Prof. Dr. D. Volkmer
Universität Augsburg, Institut für Physik
Lehrstuhl für Festkörperchemie
Universitätsstrasse 1, 86159 Augsburg (Germany)
Fax: (+49) 821-598-5955
E-mail: dirk.volkmer@physik.uni-augsburg.de

[b] Dr. A. Mavrandonakis, Prof. Dr. J. Sauer
Institut für Chemie, Humboldt-Universität zu Berlin
Unter den Linden 6, 10099 Berlin (Germany)

[c] Dr. A. Puls
Rubotherm GmbH, Universitätsstrasse 142
44799 Bochum (Germany)

[d] Prof. Dr. R. Staudt
Hochschule Offenburg, Badstrasse 24
77652 Offenburg (Germany)

[e] J. Möllmer
Institut für nichtklassische Chemie e.V. (INC)
Universität Leipzig, Permoserstrasse 15, 04318 Leipzig (Germany)

allow almost free diffusion of small molecules, in contrast to most zeolites.[8] In short, MOFs are interesting candidates for catalytic applications, with the advantages of a heterogeneous reaction course (i.e., simple catalyst recovery), while minimising the adverse effects of slow molecular diffusion, limiting reactant transport in microporous materials.

Three conceptually different approaches have been used to gain catalytically active MOFs: introducing catalytic metal centres at the nodes of the constituting secondary building units (SBUs), attaching catalytically active functional groups or coordination units at the MOF struts (i.e., the organic linkers), and embedding nanosized metal clusters within the pores of the MOF. Finely dispersed, catalytically active metal (e.g., Cu, Pd, Pt, Au) or metal oxides inside the MOF cavities can be obtained by depositing volatile organometallic precursor complexes[9] in the open MOF cavities from the gas phase or from solution,[10] enabling catalysis by MOF-encapsulated clusters. Pd@MIL-101, for instance, shows similar activity in Heck reactions as commercial catalysts[11] and CO oxidation is feasible with Au@ZIF-8[12] or Pd@MIL-101.[10a] However, sintering or agglomeration of the metal nanoparticles occurs during catalysis in some cases[13] and it seems difficult to achieve a homogeneous distribution of nanoparticles filling the internal MOF pores—as opposed to the likewise simple deposition of nanoparticles on the external surfaces of the MOF crystals.[14]

The integration of functional groups or metal coordination units into the organic linkers that constitute the struts of the framework is an attractive and straightforward approach to MOF-based heterogeneous catalysts. In several studies, metalloporphyrins,[15] Schiff base[5] or binaphthyl complexes[16] have been used as ligands. The problems related with this approach are most apparent for metalloporphyrin-based systems: first, porphyrinic MOFs featuring large open pores are highly susceptible to collapsing upon solvent removal; second, it is difficult to prevent saturation of the "free" coordination sites of the metal porphyrin, which thus become part of the framework itself; third, attempts to incorporate free-base porphyrins as struts (which would then be available for post-synthetic metallation) are generally frustrated by the tendency of the porphyrin ligand to scavenge and coordinate metal ions present in the initial MOF synthesis.

To date, the use of catalytically active metal centres positioned at the nodes of the MOF constituting SBUs has been predominantly explored for Lewis acid catalysis,[1d, 17] whereas examples of redox catalysis are rare. MOFs with copper metal centres, for instance, can catalyse the oxidative coupling of 2,6-dimethylphenol to form poly(1,4-phenylene ether). The C–O/C–C oxidative coupling selectivities are comparable to those obtained for other homo- and heterogeneous catalysts (up to 90% C–O/C–C coupling under optimised reaction conditions), and display good substrate-to-catalyst ratios as well as short reaction times.[18] By using hydrogen peroxide and MIL-101 as catalysts, selective sulfoxidation of aryl sulfides becomes feasible.[4] Iron, copper or aluminium MOFs were active catalysts for the selective oxidation of xanthene to xanthone; however, the question as to whether or not catalytic activity might be due to leaching of metal ions from the nodes of the MOFs into solution was not addressed.[19] Corma et al. have recently described the catalytic oxidation of tetralin with molecular oxygen,[20] using the Co^{II}-containing MOF ZIF-9[21] as a catalyst. They achieved 23% conversion (tetralone was the main product) after 30 h. An induction period of about 10 h existed, in which no tetralin conversion was observed. This catalyst shows no metal leaching; however, the molecular dimensions of tetralin are approx. 0.46×0.65 nm, whereas the pore aperture in ZIF-9 is only about 0.30 nm,[22] thus the intrapore diffusion of tetralin in ZIF-9 might be strongly hindered, which might indicate that the catalytic oxidation is primarily confined to the particle surface. However, it was found by several groups that ZIF-8 could accommodate larger molecules than it would be expected, based on the pore size calculated from crystallographic data;[23] a phenomenon that was already known from zeolites.[24] On the other hand, it was demonstrated that only the surface of ZIF-8 operated in the transesterification of large molecules.

To obtain hydrolytically stable cobalt(II)-based MOFs, the soft Lewis acid cobalt(II) should be coordinated to soft Lewis base atoms, such as N-heterocyclic aromatic ligands (e.g., pyridine or pyrazole ligands). The expected increase in thermodynamic stability is already gleaned by simply regarding the complete exchange of water against ammonia in tetraaquacobalt(II) ($pK = 5.5$).[25] According to the well-known Irving–Williams series,[26] the thermodynamic stability of complexes should increase, if late 3d transition-metal ions (soft Lewis acids, such as Co^{II}, Ni^{II} or Cu^{II}) are coordinated to soft Lewis base atoms, such as N-heterocyclic aromatic ligands (e.g., pyridine or pyrazole ligands). The CSD database revealed two structures based on 3,5-dimethylpyrazole (3,5-dmpz), which were suitable as SBUs for the construction of MOFs (Figure 1). These prototypic compounds are the metal complexes $[Co_4O(3,5\text{-dmpz})_6]$,[27] a structural analogue of "basic zinc acetate", $[Zn_4O(OAc)_6]$, the prototypic building unit of MOF-5-type frameworks, and $[Co^{II}(3,5\text{-dmpz})]_\infty$,[28] an infinite one-dimensional chain of tetrahedrally coordinated Co^{II} atoms. By replacing 3,5-dmpz with the linear bridging ligand 1,4-bis[(3,5-dimethyl)pyrazol-4-yl]-benzene (H_2-bdpb), which has two pyrazole groups,[29] the two MOFs MFU-1[30,31] and MFU-2 are derived from $[Co_4O(3,5\text{-dmpz})_6]$ and $[Co^{II}(3,5\text{-dmpz})]_\infty$, respectively, as outlined in Figure 1. By adjusting the reaction conditions (see the Experimental Section), both phase-pure MFU-1 and MFU-2 can be obtained in good yields by treating the ligand H_2-bdpb with a suitable Co^{II} salt under solvothermal conditions.

To follow up on our previous communication on the catalytic activity of MFU-1 employing *tert*-butyl hydroperoxide,[31] we present herein a detailed crystallographic structure analysis of both MFU-1 and MFU-2. Their catalytic activities are compared with respect to their structural features and special emphasis is placed on elucidation of structural stability and metal leaching under catalytic reaction condi-

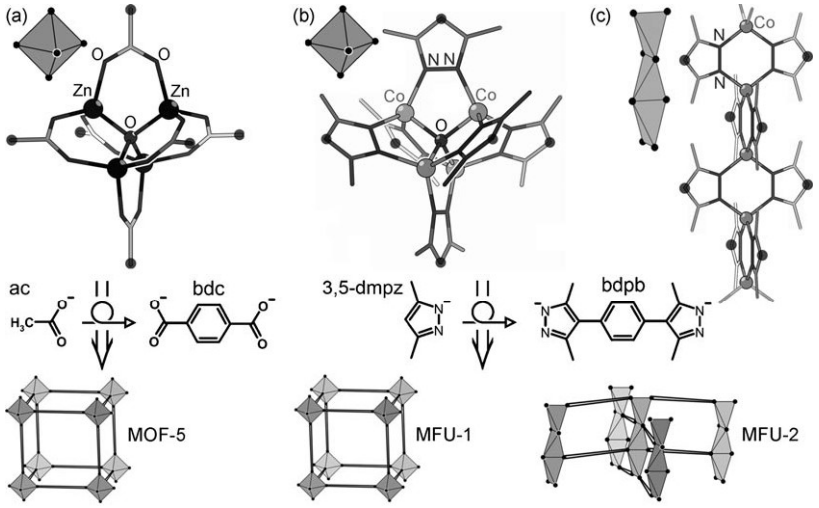

Figure 1. a) Formal derivation of MOF-5 ($[Zn_4O(bdc)_3]$[2]) from basic zinc acetate ($[Zn_4O(OAc)_6]$)[32] (bdc = 1,4-benzenedicarboxylate). b) Similar construction of MFU-1 $[Co_4O(bdpb)_3]$ from a (pseudo-)octahedral complex $[Co^{II}{}_4O(3,5\text{-dmpz})_6]$[27] ($H_2$-bdpb = 1,4-bis[(3,5-dimethyl)-pyrazol-4-yl]benzene). c) Derivation of MFU-2 from catenapyrazolato cobalt(II).[28] The MOFs are generated from the corresponding SBUs by connecting the points of extension (indicated by grey dots) with 1,4-phenylene units.

tions. The local coordination environment and the oxidation state of the Co centres are investigated by means of X-ray absorption spectroscopy at the Co K edge and changes occurring upon catalysis are analysed, revealing details of the presumed catalytic reaction. To elucidate the interaction of both frameworks with molecular oxygen, the isosteric heats of O_2 adsorption are determined. Moreover, both compounds are studied by temperature-programmed oxidation (TPO). First results from DFT calculations are presented to support our conclusions drawn from structural and spectroscopic studies, gleaning further details about the activation of oxidants by pyrazolate-based MOFs containing cobalt(II). As a preliminary summary, activation of molecular oxygen by MFU-1 is feasible (in contrast to MFU-2), thus enabling heterogeneous catalytic oxidation reactions under mild reaction conditions. Table 7 at the end of this article summarises the key data of the results presented in the following sections.

Results and Discussion

Single crystals of MFU-1 and MFU-2 were grown slowly under solvothermal conditions by treating the ligand H_2-bdpb with cobalt chloride or cobalt nitrate, respectively, in DMF at 120 °C (see the Experimental Section). For a more efficient bulk synthesis of phase-pure compounds, we employed a microwave system (focused microwave irradiation with 300 W output power at a frequency of 2.46 GHz), which reduced the reaction time required from several days to a few minutes and significantly increased the yield. Based on results from X-ray powder diffraction (see the Supporting Information), these microcrystals are structurally identical to those obtained from solvothermal synthesis and show the same porosity (as proven by argon BET measurements), albeit the crystals obtained from microwave synthesis are significantly smaller and more uniform in size.[33] The final crystallographic data and details of the refinement are summarised in Table 1.

Crystallography of MFU-1: Crystallographic data sets for MFU-1 were obtained from different crystal specimens suitable for single-crystal X-ray diffraction by employing both $Cu_{K\alpha}$ and $Mo_{K\alpha}$ radiation. To remove occluded DMF solvent molecules, the suspension of crystals was heated at reflux multiple times with chloroform and the crystals were kept for at least 12 h in high vacuum ($p < 10^{-4}$ mbar). The crystallographic data from six independent measurements uniformly showed a large residual

Table 1. Crystallographic data for MFU-1 and MFU-2.

	MFU-1	MFU-2
formula	$C_{48}H_{48}Co_4N_{12}O$ [$Co_4O(C_{16}H_{16}N_4)_3$]	$C_{16}H_{16}CoN_4$ [$Co(C_{16}H_{16}N_4)$]
M_r	1044.70	323.26
crystal system	cubic	tetragonal
space group	$P\bar{4}3m$ (no. 215)	$P4_2/ncm$ (no. 138)
a [Å]	15.7904(2)	18.6070(8)
b [Å]		18.6070(8)
c [Å]		7.1635(5)
α [°]	90	90
β [°]	90	90
γ [°]	90	90
V [Å^3]	3937.13(9)	2480.2(2)
Z	1	4
$F(000)$	536	668
ρ_{calcd} [g cm^{-3}]	0.441	0.866
λ [Å]	0.71073	1.54184
μ [mm^{-1}]	0.429	5.409
crystal size [mm]	0.073 × 0.071 × 0.070	0.054 × 0.052 × 0.016
T [K]	120(2)	120(2)
Θ range [°]	3.65–29.34	3.36–58.88
min/max h	−20/21	−20/11
min/max k	−21/18	−17/20
min/max l	−20/19	−7/5
collected reflns	17696	4583
unique reflns	1975	922
reflns with $I > 2\sigma(I)$	1295	444
params/restraints	52/1	61/6
GoF on F^2	0.961	0.942
R_1 (on F, $I > 2\sigma(I)$)	0.0529	0.0856
wR_2 (on F^2, all data)	0.1390	0.2274
max/min $\Delta\rho$ [e Å^{-3}]	0.551/−0.332	1.086/−0.911

electron density in the void regions of the crystal lattice. The residual electron density was quite diffuse owing to the strong positional disorder of residual DMF molecules occluded in the lattice voids of MFU-1. Thus, all atom coordinates gleaned from the first structure solution proved to be unstable in subsequent refinement cycles and collapsed to chemically unreasonable structures in all attempts. PLATON/SQUEEZE[34] was employed to correct the initial X-ray reflection data set for those regions containing highly disordered components. A potential solvent volume of 2528 Å^3 (corresponding to approximately 20 DMF molecules),[35] containing 241 electrons was found. A further interpretation of the electron density maxima found in the void regions of MFU-1, which might indicate partial interpenetration, is given in the Supporting Information.

Structure solutions of all data sets invariably suggested space group $P\bar{4}3m$, although subsequent refinement cycles clearly showed the presence of unresolved electron density maxima in close proximity to the {Co_4O} units of the framework. Initial attempts to assign this residual electron density to μ_3-bridging ligand species, such as O^{2-} or OH^-, failed. The refinement was neither stable (even if the occupancy factors of this crystallographic site were freely refined), nor could we find further support from spectroscopic studies in favour of this structural model. Nevertheless, based on theoretical models of the MFU-1 crystal lattice, the unassigned electron density and the observed disorder phenomena can be explained in terms of 1) structural linkage isomerism, 2) rotational disorder of interconnecting 1,4-phenylene units and 3) chiral distortion of the {$Co_4O(3,5\text{-dmpz})_6$} SBUs, leading to a deviation of the real structure of MFU-1 from the idealised model, represented by the highly symmetric solution in space group $P\bar{4}3m$, as shown in Figure 2.

In the chosen (achiral) space group, the phenylene moieties of the bridging bdpb ligand occupy two alternative positions with 50% probability each. The bdpb ligands and {Co_4O} units are linked into a cubic network (Figure 2) of low density ($\rho_{calcd} = 0.44\ g\,cm^{-3}$). The structure of MFU-1 is similar to that of MOF-5, which has a CaB_6-type framework topology. It encloses (pseudo)octahedrally shaped {$Co_4O(3,5\text{-dmpz})_6$} SBUs reminiscent of the {$Zn_4O(CO_2)_6$} SBUs in MOF-5 and phenylene rings representing the edges of the cubic six-connected CaB_6 net. The framework has three-dimensional intersecting channels that encompass almost spherical voids with a volume of about 2528 Å^3 each. The square windows of MFU-1 are apertures of 9.0 Å (distance between opposing phenylene units regarding the van der Waals radii).[22] A structurally related MOF network constructed from μ_4-oxo-bridged tetrazinc units and 3,3′,5,5′-tetramethyl-4,4′-bipyrazolate linkers has recently been reported.[36]

As previously mentioned, all structure solutions and refinements (even those performed in the space group P_1) gave rise to a strong residual electron density, the maxima of which had the same distance to the central oxygen atom as the cobalt ions (Figure 3). This electron density can be explained in terms of two different {Co_4O} tetrahedra that

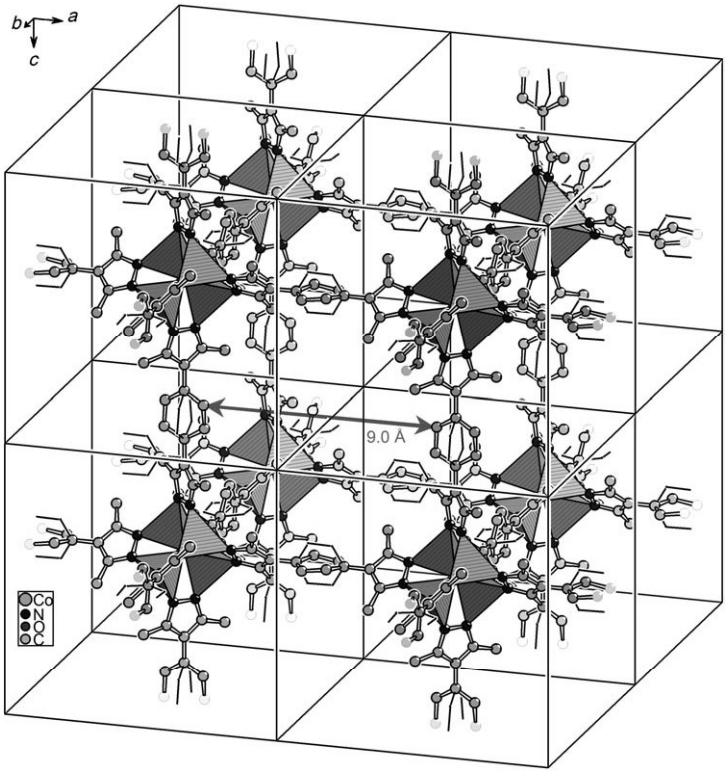

Figure 2. Crystal packing diagram of MFU-1. {$CoON_3$} coordination units are represented as polyhedra. The phenylene moieties of the bridging bdpb ligands occupy two alternative (symmetry equivalent) positions with equal probability, one of which is displayed in the graphics by thin black lines. Approximately 20% of all {$Co_4O(dmpz)_6$} units are placed at structurally inverted positions, for which the central oxygen atoms act as centres of symmetry. (Only major disorder components are shown; hydrogen atoms are omitted for clarity.)

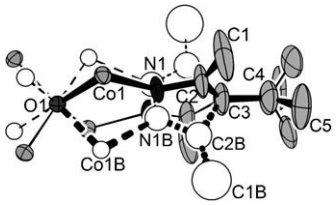

Figure 3. An ORTEP representation and the numbering scheme of the asymmetric crystallographic unit of MFU-1. Atoms of the anisotropically refined main component (O1, Co1, N1, C1–C5) are represented by thermal displacement ellipsoids connected with bold (filled) lines, representing bonds. The minor disorder component (Co1B, N1B, C1B, C2B; 20% probability) is represented by open circles and broken lines. Additionally, symmetry generated atoms (from both disorder components) are connected by thin lines.

are virtually superimposed by inversion: the oxygen atom (O1) representing the centre of symmetry, thus leads to an observed pseudo-cubic arrangement of electron density maxima assigned to the positions of cobalt atoms (Co1 and Co1B), as shown in Figure 3. The refinement reveals that 20% of the {Co_4O} tetrahedra in MFU-1 are inverted through their central oxygen atom as a statistically distributed minor disorder component.

As an illustration of the linkage isomerism, an excerpt of a lattice plane of MFU-1 is shown in Figure 4a, in which the foremost $\{Co_4O(3,5\text{-dmpz})_6\}$ SBU is symbolised by an open octahedron. This unit can be inverted (by employing the central oxygen atom as the symmetry centre), as shown in Figure 4b, and the altered unit can be re-inserted into the crystal lattice without introducing any kinds of steric repulsion or strain. Thus, at first approximation there should be no energetic differences between the different lattice isomers emerging from structural differences (neglecting entropic factors, however).

All X-ray data sets recorded from MFU-1 single crystals so far indicate a strong preference for a uniform orientation of SBUs such that the (occasional) occurrence of inverted units (the refined ratio between both components is 0.8:0.2) leads to a relatively strong residual electron density that is ascribed to the cobalt centres located at the alternative positions of the minor component. A possible explanation for the experimental finding that 20% of the $\{Co_4O(3,5\text{-dmpz})_6\}$ units are statistically inverted might be as follows: There are two highly symmetrical space groups in which the MFU-1 structure might be represented, namely, $P\bar{4}3m$ or $F\bar{4}3m$. In the space group setting of $P\bar{4}3m$, all SBUs are symmetry related by simple translation. This arrangement is possible only if the pyrazole ring systems at both ends of the same bridging ligand are orthogonal to each other (Figure 5, top).

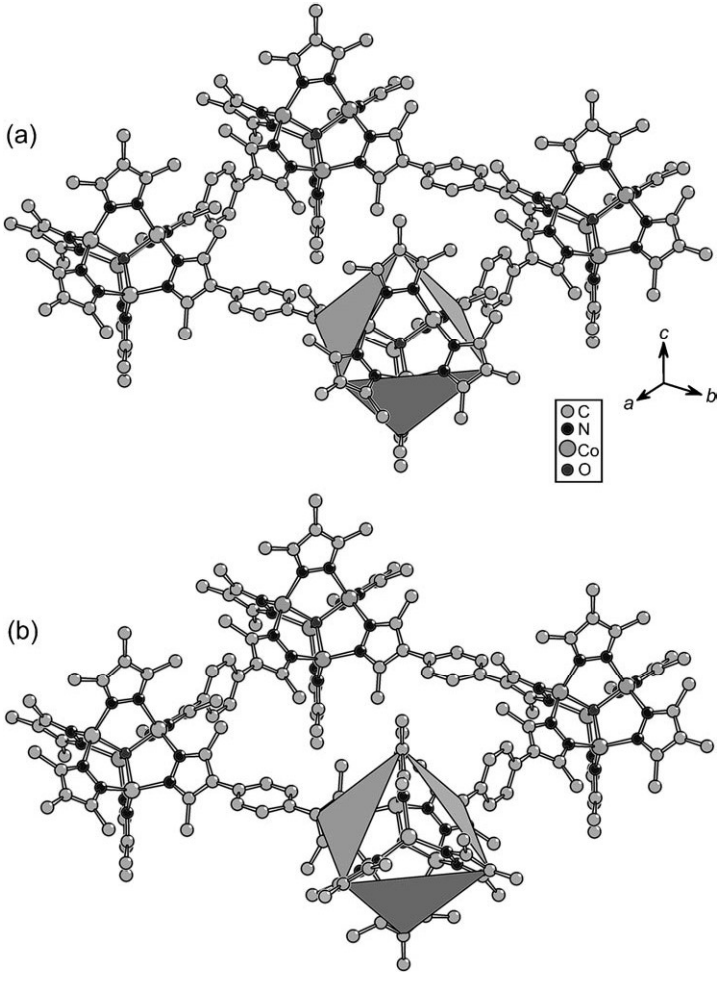

Figure 4. Structural lattice isomerism of $\{Co_4O(3,5\text{-dmpz})_6\}$ SBUs. a) Adjacent SBUs are symmetry related by simple translations. b) Inversion (by employing the central oxygen atom as the symmetry centre) of a single $\{Co_4O(3,5\text{-dmpz})_6\}$ SBU symbolised by an open octahedron. Based on the electron density distribution in MFU-1, the statistical linkage isomerism is present at approximately 20% of the $\{Co_4O(3,5\text{-dmpz})_6\}$ SBUs.

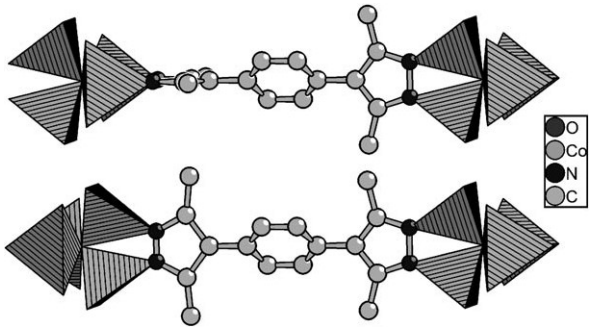

Figure 5. Different arrangements of adjacent $\{Co_4O(3,5\text{-dmpz})_6\}$ SBUs forced by the space group symmetry settings in the space group $P\bar{4}3m$ (top) and $F\bar{4}3m$ (bottom). $\{CoN_3O\}$ coordination units are drawn as polyhedra.

In the space group $F\bar{4}3m$ (the one most often used to represent MOF-5), on the other hand, adjacent SBUs cannot be brought to congruence by a simple translation. Adjacent SBUs connected to the same linker have to be inverted before translation and thus 50% of the $\{Co_4O(3,5\text{-dmpz})_6\}$ nodes in the space group setting $F\bar{4}3m$ are inverted, necessitating, however, a parallel arrangement of pyrazole rings at both ends of the bridging ligand, as shown in Figure 5 (bottom).

By assuming that the energetic differences between both conformers of the bridging ligand are negligible, a statistically equally weighted distribution should be observed. Thus, a 1:1 occurrence of both conformers would be equivalent to the fact that inversion should occur for 25% of the $\{Co_4O(3,5\text{-dmpz})_6\}$ units; this comes close to the 20% of inversion disorder experimentally determined for the structure solution in space group $P\bar{4}3m$. Nevertheless, it should be kept in mind that the shape and packing density of occluded solvent molecules may have a strong influence on this conformational disorder phenomenon.

A refinement in the space group $F\bar{4}3m$ (by using a unit cell with doubled cell constants) revealed a statistical disorder of the inverted $\{Co_4O(dmpz)_6\}$ node as well. By using this space group, the main disorder compound also displays adjacent $\{Co_4O\}$ units that are symmetry related by simple translation. This finding further supports a statistical disorder of the $\{Co_4O\}$ units, showing that no higher crystallographic order is present. However, not all atoms of the minor disorder compound can be found in the space group $F\bar{4}3m$.

Apart from the structural disorder brought into the MFU-1 crystal lattice by linkage isomerism, the finally converged structure refinement showed some additional unusual crystallographic properties, such as physically doubtful anisotropic displacement parameters for the methyl substituents of the pyrazolate moieties (atom C1, Figure 3). A closer inspection revealed that this artefact was presumably due to the fact that the $\{Co_4O(3,5\text{-dmpz})_6\}$ SBUs were chirally distorted (T rather than T_d point group symmetry) with both possible enantiomers equally distributed in the crystal lattice (Figure 6). The electron density thus represents an equally

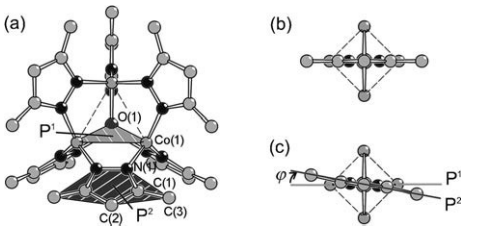

Figure 6. a) Ball-and-stick model of the complete and fully T_d symmetrical $\{Co_4O(pz_6)\}$ SBU of MFU-1. A chiral distortion of this unit is characterised by the interplanar angle ϕ between the two least-squares planes through the atom centres O(1)-Co(1)-Co(1)′ (P^1) and N(1)-C(1)-C(3)-C(2)-C(3)′-C(1)′-(N(1)′ (P^2). Simplified representations of the SBU. In the model showing T_d symmetry (b), the interplanar angle ϕ is 0°, whereas the T-symmetric chiral SBU (c) is characterised by a finite angular ϕ value.

weighted superposition of two different enantiomers that show significant structural deviations from T_d point group symmetry. The chiral distortion of the $\{Co_4O(3,5\text{-dmpz})_6\}$ SBUs of MFU-1 can be rationalised in terms of the steric repulsion between methyl substituents of the 3,5-dmpz ligands. As Figure 6c demonstrates, the distortion should lead to deviation of atomic positions of the coordinated pyrazolate moieties from idealised T_d symmetry (which itself is imposed by the symmetry settings of space group $P\bar{4}3m$). This chiral distortion is apparent in the crystal structure of $[Co_4O(3,5\text{-dmpz})_6]$,[27] in which the idealised T_d symmetry of each individual and discrete coordination unit is reduced to chiral T point group symmetry (Table 2).

DFT calculations augmented by a semi-empirical dispersion term (denoted as DFT+D) were performed to investigate the conformation of the pyrazole rings around the $\{Co_4O\}$ core. Two different initial conformations were taken into account, corresponding to a local T_d and T symmetry around the SBU of MFU-1. However, when building a periodic model of the crystal structure, the symmetry of the cell has to be reduced to T because the phenylene moieties can occupy only one of the two symmetry equivalent positions (see Figure 2).

Table 2. Lattice parameters $a=b=c$ [Å], selected bond lengths [Å] and angles [°] in MFU-1 and $[Co_4O(3,5\text{-dmpz})_6]$.[27]

	MFU-1 (exptl)	MFU-1 (DFT+D)[a]	$[Co_4O(3,5\text{-dmpz})_6]$[27]
$a=b=c$	15.790	15.804	
Co–O	1.95	1.96	1.94–1.95
Co–N	1.98	1.97	1.99–2.02
Co-O-Co	109.5	109.5	108.1–111.8 (Ø 109.5)
N-Co-O	98.2	97.6	96.6–100.2 (Ø 98.3)
N-Co-N	118.0	118.3	114.1–122.1 (Ø 118.0)
ϕ	0.0	1.9–4.6	0.1–6.4 (Ø 3.9)

[a] DFT+D = DFT calculations augmented by a semi-empirical dispersion term.

The DFT+D results show that the conformation of the pyrazole rings around the $\{Co_4O\}$ is flexible. Optimization of the two initial conformations results always in structures with a chiral distortion. The energy minimum for the interplanar ϕ angle (as defined in Figure 6) found for the infinite network is between 1.9 and 4.6° (Table 2), corresponding to local T symmetry, but since the energy changes connected with these angle changes (less than 0.4 kJ mol^{-1}) are within the numerical accuracy limits of the calculations, we cannot rule out that the minimum is at 0°. This suggests that, even at a temperature around 100 K, MFU-1 can adopt various possible conformations. The flatness of the potential explains the observed elongation of the thermal ellipsoid in the single-crystal X-ray structure analysis. Thus, the long-range crystallographic order of MFU-1 seems to be appropriately represented in the setting of the achiral space group $P\bar{4}3m$.

Crystallography of MFU-2: The crystallographic structure analysis of MFU-2 is based on solvent-free crystals. MFU-2 crystallises in the tetragonal crystal system in space group $P4_2/ncm$ (no. 138). The asymmetric unit of the unit cell is displayed in Figure 7. The phenylene moieties of the bridging bdpb ligands occupy two alternative positions with 87 (C5) and 13% (C5B) probability.

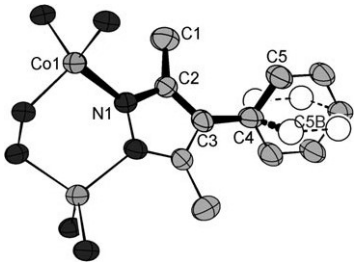

Figure 7. ORTEP representation and numbering scheme of the asymmetric unit present in crystalline MFU-2. The main component is drawn with solid lines as bonds and front ellipses for the atoms, whereas the minor disorder component (C5B, 13% probability) is drawn with bold broken lines as bonds and open ellipses as atoms. Symmetry-related atoms are connected by thin lines.

The framework contains quadratic tunnels running through the crystal, consisting of 1D chains of cobalt(II) ions bridged by dianionic bdpb ligands that extend along the c axis of the crystal lattice. A similar structure constructed from 1D chains of cobalt(II) ions bridged by linear tetrazolate based linkers has been recently reported.[37] Each Co^{II} centre is coordinated by four nitrogen donor atoms stem-

ming from different ligands. The local $\{CoN_4\}$ coordination site adopts D_{2d} point group symmetry, with all Co–N bond distances being equal (1.992(5) Å), and two out of six N-Co-N′ angles being slightly narrowed (106.6(3)°, as opposed to four widened angles (110.9(1)°). Adjacent cobalt(II) centres are bridged by bdpb ligands to form 6-membered $\{Co_2N_4\}$ rings with a Co···Co distance of 3.5818(3) Å resulting in a PtS-type framework topology.[38] Figure 8 shows the quadratic channels of 18.61 Å (lengths of the diagonal) in MFU-2 running along the *c* axis. The square channels in MFU-2 have apertures of 6.4 Å (distance between opposed phenyl rings regarding the van der Waals radii of 1.7 Å for the carbon atoms).[22]

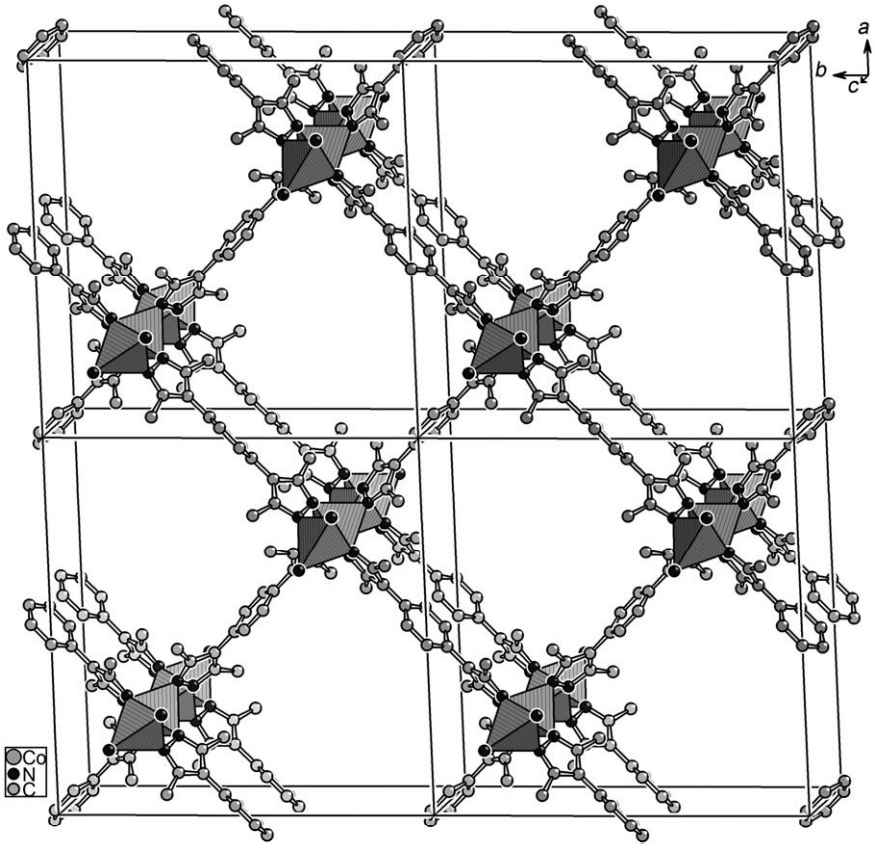

Figure 8. Crystal-packing diagram of MFU-2. $\{CoN_4\}$ coordination units are represented as polyhedra. Hydrogen atoms are omitted for clarity. Only the major rotational disorder component out of two alternative positions of the benzene moieties is shown.

PLATON/SQUEEZE[34] was used to further analyse the void region of MFU-2 (but no correction of the scattering intensities was performed). A potential solvent volume of 1164 $Å^3$ was found (corresponding to approximately 8 DMF molecules).[35]

The structure of MFU-2 is related to that of MFU-3,[39] which possesses the same structural motif of cross-linked infinite 1D chains of cobalt(II) ions, the bridging ligands, however, are composed of simple pyrazolate rather than 3,5-dimethylpyrazolate moieties. The different substitution pattern of the coordinating pyrazolate ligands leads to marked structural differences. Looking down the chain of cobalt(II) ions in MFU-3, the set of planes running through adjacent pyrazole ring systems are strictly orthogonal to each other. In MFU-2, on the other hand, the least-squares planes through opposite pyrazole rings of the same coordination unit display a torsional distortion as a result of the steric interactions between adjacent methyl substituents, thus leading to an interplanar angle of 29° (Figure 9, as opposed to 0° in MFU-3). As a result of sterically less-encumbered coordination geometry, MFU-3 shows a pronounced framework flexibility and thus a breathing effect, as revealed by a formal type IV gas sorption isotherm, whereas MFU-2 is a rigid network displaying a type I gas sorption isotherm.

Thermal stability: Investigations on the thermal stabilities of MFU-1 and MFU-2 were performed by combining thermogravimetric analysis (TGA; samples exposed to flowing nitrogen atmosphere) and variable-temperature X-ray powder diffraction (VTXRPD) (samples kept in static air). Both untreated (as-synthesised) samples and samples suspended in CH_2Cl_2 for 24 h, followed by drying in vacuum, were examined by TGA. Additionally, temperature-programmed oxidation (TPO) was carried out by employing O_2 gas. For the as-synthesised samples, the TGA of MFU-1 showed a loss of occluded solvent molecules in the temperature range 75–225 °C to yield the solvent-free crystal form (weight loss: 11.9 %; expected 12.3 % for complete loss of DMF from MFU-1·2 DMF). Whereas the for-

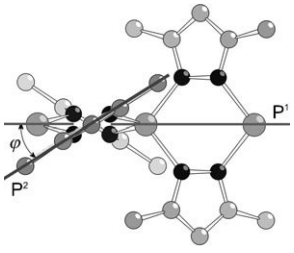

Figure 9. Distortion of the pyrazolate units, characterised by the interplanar angle ϕ between the two least-squares planes through the cobalt atoms of two adjacent Co chains (P^1) and the pyrazolate rings (P^2).

mulation MFU-1·2DMF is in agreement with the observed weight loss and the elemental analyses, the solvent-accessible voids in the crystal lattice could, in principle, take up to as many as 20 DMF molecules per formula unit. Whereas a slight reduction of solvent molecules in the voids of MFU-1 might be due to filtering, such an enormous difference between observed and expected weight loss might hint that partial interpenetration occurs. The BET surface area and pore volume in gas sorption experiments are lower than those calculated from the crystallographic structure as well, further supporting a partial interpenetration of the framework.

No further weight loss occurred below 340 °C; ligand molecules from the framework were degraded in the temperature range 340–1100 °C (weight loss: 44.1 %; expected 66.5 % for complete loss of bdpb). Upon suspending MFU-1 in CH_2Cl_2 for 24 h, followed by drying in vacuum, the initially occluded DMF molecules were removed completely, which was indicated by a residual weight loss of 2.9 % in the temperature range 30–195 °C, with no further weight loss occurring below 340 °C. Accordingly, the VTXRPD patterns indicate that the MFU-1 framework was stable up to 270 °C in static air (see the Supporting Information). TGA of MFU-2 indicated a loss of solvent molecules up to 260 °C (weight loss: 21.8 %; expected 18.5 % for complete loss of DMF from MFU-2·DMF), and ligand molecules from the framework were degraded in the temperature range 340 °C-470 °C (weight loss: 54.2 %; expected 66.6 %). Whereas the formulation MFU-2·DMF is consistent with the composition gleaned from elemental analysis, the void volume of MFU-2 generally would be able to accommodate two DMF molecules per unit cell, indicating a partial loss of DMF molecules during the workup procedure. The VTXRPD patterns indicated that the framework of MFU-2 was stable up to 300 °C (see the Supporting Information). Furthermore, these results showed that both MOF frameworks were stable upon complete removal of solvent molecules.

To probe thermal stabilities and redox behaviour of both frameworks in reactive gas atmospheres, TPO experiments were performed (Supporting Information). In all experiments, fresh samples of MFU-1 and MFU-2 were heated at reflux with CH_2Cl_2 prior to drying in high vacuum. The samples were then kept at 200 °C for 2 h to remove residual solvent molecules (observed weight loss: 2 %). By using TPO in diluted oxygen (1000 ppm of oxygen in helium), MFU-1 showed reaction with oxygen starting at 100 °C and a release of CO_2 and H_2O (indicative of decomposition) at 140 °C and above. In contrast to MFU-1, MFU-2 showed no sign of reaction with oxygen or decomposition below 230 °C, indicating a higher stability (and thus a lower reactivity) towards molecular oxygen. Moreover, MFU-1 showed a colour change from blue to green in an oxygen atmosphere after reaching a temperature of approximately 140 °C, which was due to an additional absorption band occurring at 410 nm. This colour change might be tentatively ascribed to the oxidation of Co^{II} to Co^{III} ions under retention of the tetrahedral coordination environment.[40] Furthermore, the sample treated at 140 °C in oxygen showed changes in the IR spectrum (additional bands around 1600–1700 cm^{-1}, indicating the presence of carboxylate and/or amide groups), and only an amorphous product in the XRD powder patterns (see the Supporting Information). No spectral or structural changes were discernible for MFU-2 in TPO experiments upon heating the sample up to 230 °C.

Oxygen isosteric heat of adsorption: To investigate the interaction of both framework compounds with molecular oxygen, the isosteric heat of adsorption for different oxygen loadings on MFU-1 and MFU-2 was examined, employing a magnetic suspension balance. Prior to sorption experiments all samples were pre-treated at 200 °C for 2 h to remove residual solvent molecules (observed weight loss: 2 %).

For a correct calculation of the isosteric heat of adsorption from the measured adsorption isotherm, a minimum of at least three isotherms are necessary.[41] Therefore, oxygen adsorption isotherms for MFU-1 and MFU-2 were measured gravimetrically at 298, 323 and 343 K and for pressures up to 4 MPa. The executed loadings ranging from 0.01–1 mmol g^{-1} are equivalent to 0.04–4 molecules of oxygen per Co atom. All isotherms are displayed in Figure 10 for MFU-1 and Figure 11 for MFU-2.

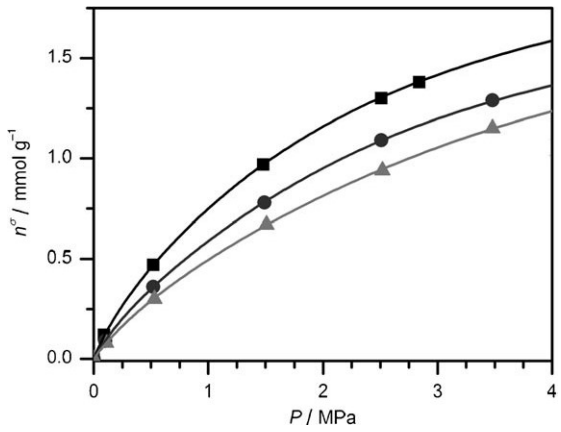

Figure 10. Oxygen adsorption isotherms of MFU-1 at 298 (■), 323 (●) and 343 K (▲) (lines are from fitted virial equation).

Beginning at 120 °C (393 K), MFU-1 in oxygen shows a very slow but steady decrease of mass without reaching equilibrium even after 72 h. X-ray powder diffraction indicates that CoO and Co_3O_4 are obtained as final products. Thus, temperatures higher than 343 K were avoided. We attribute this steady weight loss to the activation of molecular oxygen at higher temperatures, which subsequently leads to oxidation of the organic part of the framework.

The isosteric heat of adsorption, q_{st}, was determined by fitting a virial-type equation to the adsorption isotherms. The ln(p) values for a given amount adsorbed (n) were calculated from the linear regressions determined from the virial equation analysis by using Equation (1):[42]

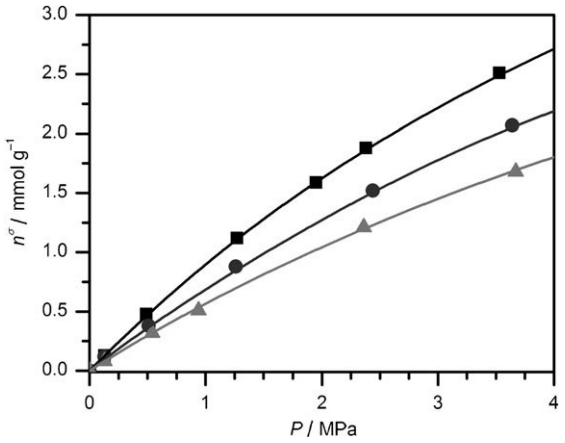

Figure 11. Oxygen adsorption isotherms of MFU-2 at 298 (■), 323 (●) and 343 K (▲) (lines are from fitted virial equation).

$$\ln(p/n) = A_0 + A_1 n + A_2 n^2 + A_3 n^3 + \ldots \quad (1)$$

in which p is the pressure, n is the amount of adsorbed oxygen and A_0, A_1 and so forth are virial coefficients. A_0 is related to adsorbate–adsorbent interactions and at low surface coverage the Henry's Law constant (K_H) is equal to $1/\exp(A_0)$.[42] The q_{st} values were subsequently determined by using a modified version of the Clausius–Clapeyron equation [Eq. (2)]:

$$\left(\frac{-q_{st}}{RT^2}\right) = \left(\frac{\partial \ln p}{\partial T}\right)_N \quad (2)$$

The q_{st} values for MFU-1 and MFU-2 are shown in Figures 12 and 13, respectively. From the gravimetric oxygen adsorption isotherms, we thus derive an isosteric heat of adsorption of (-11.1 ± 0.9) kJ mol^{-1} for MFU-1 and (-8.5 ± 0.9) kJ mol^{-1} for MFU-2, throughout the entire range of coverage explored. On the other hand, at pressures above

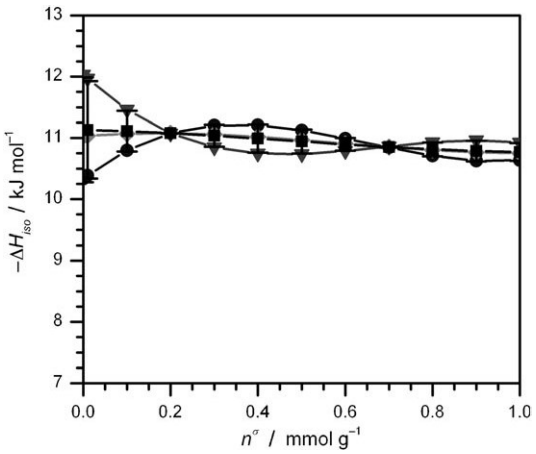

Figure 12. Isosteric heat of adsorption of O_2 on MFU-1 (11.1(9) kJ mol^{-1} at $n^{\sigma} \rightarrow 0$) at 298–323 (●), 298–343 (◆) and 323–343 K (▼). The average values are also shown (■).

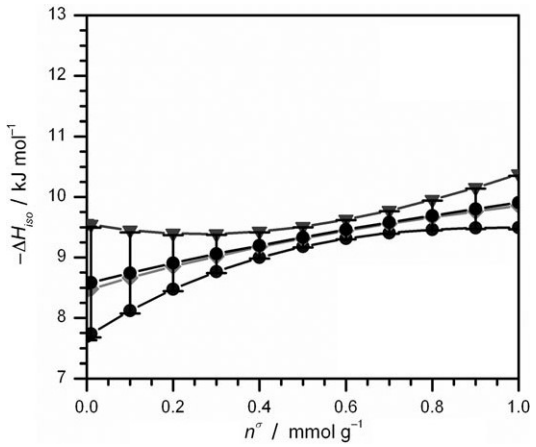

Figure 13. Isosteric heat of adsorption of O_2 on MFU-2 (8.5(9) kJ mol^{-1} at $n^{\sigma} \rightarrow 0$) at 298–323 (●), 298–343 (◆) and 323–343 K (▼). The average values are also shown (●).

0.5 MPa, the amount of oxygen adsorbed is lower for MFU-1 when directly compared with MFU-2.

For an analysis of the adsorbate–adsorbent interaction, the K_H value at low surface coverage is an ideal parameter.

Table 3. Parameters of the virial equations and K_H for MFU-1 and MFU-2.

T [K]	A_3	A_2	A_1	A_0	K_H [mmol MPa^{-1} g^{-1}]
MFU-1					
298	0.3207	−0.8145	1.2916	−0.3561	1.4278
323	0.5004	−1.1645	1.4714	−0.0334	1.0340
343	0.3820	−0.9224	1.3236	0.2279	0.7962
MFU-2					
298	−0.0018	0.0261	0.0783	0.0200	0.9802
323	0.0282	−0.0920	0.2227	0.2603	0.7708
343	0.0133	−0.0299	0.1933	0.4678	0.6264

Table 3 contains all fitting parameters of the virial equation, including K_H. At each temperature a higher K_H was observed for MFU-1 than MFU-2, indicating a stronger binding of oxygen with the binding sites of MFU-1, corresponding with the higher isosteric heat of adsorption.

Whereas MFU-1 ($\Delta H_{iso} = -11.1$ kJ mol^{-1}) showed a slightly increased isosteric heat of adsorption than MFU-2 ($\Delta H_{iso} = -8.5$ kJ mol^{-1}), somewhat larger values of ΔH_{iso} were found for Co-exchanged zeolites and a Co-based MOF (-15.1 up to -18.5 kJ mol^{-1}).[43] The range of observed values clearly indicated the presence of van der Waals complexes and their slight variations may have indicated different degrees of shielding of the Co^{II} binding sites by the organic linkers.

Despite the implied formation of a van der Waals complex at the indicated temperatures, MFU-1 showed a measurable reaction with oxygen above 120 °C in TPO and during the measurement of the gravimetric oxygen adsorption isotherms. In contrast, MFU-2, according to TPO measurements, seems to be inert up to a temperature of at least 230 °C (see the Supporting Information). A possible explan-

ation for these different reactivities towards molecular oxygen is that the cobalt(II) ions in both frameworks are sterically shielded by the organic linkers and thus poorly accessible to coordinating molecules. However, whereas the cobalt centres in MFU-2 are completely shielded, two potentially accessible coordination sites in MFU-1 should still exist, as gleaned from space-filling models (Figure 14). The

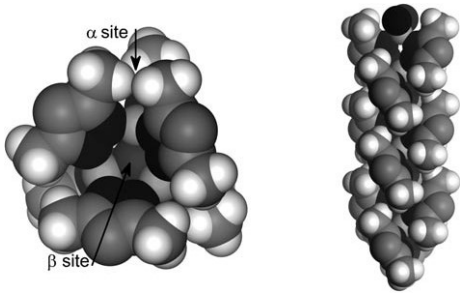

Figure 14. Space-filling models of characteristic coordination units in MFU-1 (left) and MFU-2 (right), illustrating the steric shielding of the metal ions by the ligand.

α site of MFU-1 (Figure 14) may be considered to be the "natural" coordination site of the cobalt(II) centres because binding of a monodentate ligand would lead to a change of coordination state from tetrahedral to trigonal bipyramidal, which, according to a ligand-field theoretical approximation, should lead to an energy gain.[44]

However, as can be seen from Figure 14, the α sites in MFU-1 are completely sterically shielded by the close-packed methyl substituents and a widening of the cobalt coordination shell would thus require a huge distortion of the $\{Co_4O(3,5\text{-dmpz})_6\}$ SBU, which might still be feasible for a molecular complex, but owing to symmetry restraints will be almost impossible if the same coordination unit is embedded in a 3D crystalline framework. Apart from α sites, each SBU in MFU-1 displays four easily accessible β sites, which might serve the purpose of ligand coordination. However, if binding of a ligand occurred in a symmetrical fashion, that is, if the ligand coordinated to three cobalt(II) centres in μ_3-bridging mode, the individual coordination environments of the cobalt centres would become largely distorted. This would constitute an energetically unfavourable situation, that is, a strained or "entatic state".[45] As an alternative to this energetically unfavourable situation, a rapid outer-sphere electron transfer might take place from the $\{Co_4O\}$ cluster core towards an oxidising substrate, alleviating the problem of direct coordination. To examine the putative free coordination sites in MFU-1, the compound was treated with test molecules that were commonly considered to be "strong" ligands in cobalt(II) coordination chemistry. In essence, the UV/Vis spectrum of MFU-1 showed no change if the compound was exposed to CO atmosphere at room temperature; similarly, treating a MFU-1 suspension with a solution of cyanide ions in methanol (using tetraethylammonium cyanide) gave no indication of spectral changes and the same behaviour was observed when the sample was kept in pure *tert*-butyl isonitrile (see the Supporting Information). These experimental observations are in sharp contrast to other Co^{II}-based MOFs with more accessible metal sites,[43] which leads us to conclude that coordinative binding of ligands in MFU-1 becomes largely suppressed owing to steric shielding of the cobalt centres and symmetry constraints imposed by the tetranuclear coordination units.

Figure 15 shows the DFT+D optimised structures of a van der Waals and an η^2-superoxo complex of O_2 with MFU-1. For the van der Waals complex, the predicted heats of adsorption[46] at 298 K are −7.7 (PBE+D) and

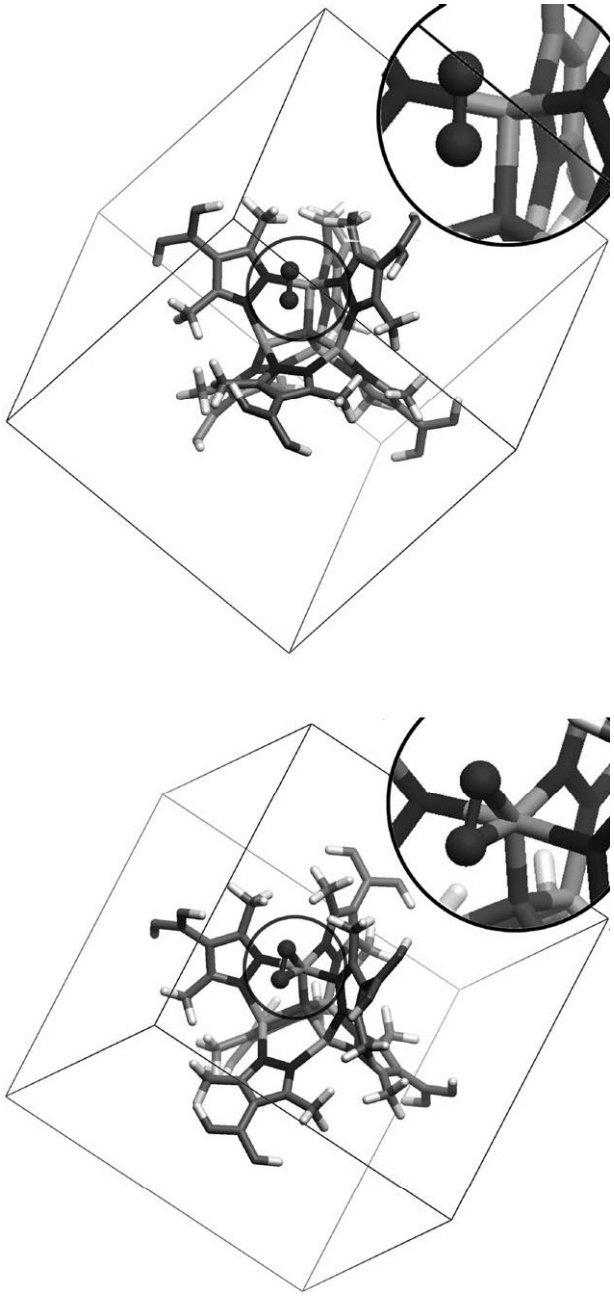

Figure 15. Structure of the van der Waals (top) and superoxo complexes (bottom) of O_2 with a metal SBU obtained by DFT (PBE+D) for the periodic MFU-1 structure.

$-8.9\ kJ\,mol^{-1}$ (B3LYP+D), close to the experimental isosteric heat of adsorption ($(11.1\pm0.9)\ kJ\,mol^{-1}$). Whereas the predicted stabilities of the van der Waals complex, employing different functionals, are in quantitative agreement, they are controversial for the η^2-superoxo–Co^{III} complex. The PBE+D functional predicts it to be the most stable complex with $\Delta H(298\ K)=\Delta H_{iso}=-52.7\ kJ\,mol^{-1}$, whereas the B3LYP+D estimate is $+64.9\ kJ\,mol^{-1}$. Presently there are no means to decide which functional is right in its prediction; this is frequently the case with multinuclear transition-metal compounds.[47] The B3LYP+D result would be in agreement with the experimental observation that below 120 °C only a van der Waals complex is observed, whereas the PBE+D result implies that formation of the η^2-superoxo–Co^{III} complex is prevented by an energy barrier. A detailed outline of the DFT calculations will be given elsewhere.[46]

BET/gas sorption: Both MOF compounds exhibit permanent porosity, which has been confirmed by argon gas sorption. Prior to measurements, the samples were heated at reflux several times in CH_2Cl_2 to exchange the DMF molecules with the more volatile solvent. The samples were subsequently heated at 150 °C for 30 h in high vacuum. The sorption isotherms of MFU-1 and MFU-2 obtained with argon gas reveal type I sorption behaviour for both substances, which is characteristic of microporous solids (see the Supporting Information). The adsorption data was analysed in the appropriate pressure range[48] to give BET surface areas of 1525(51) m^2g^{-1}[49] for MFU-1 obtained by solvothermal synthesis and 1485(50) m^2g^{-1} for MFU-1 from microwave synthesis (see the Supporting Information). By using a sample from microwave synthesis, the BET surface was reduced to 1018(33) m^2g^{-1} after catalysis, employing *tert*-butyl hydroperoxide as described below. For MFU-2, BET surface areas of 1474(50) m^2g^{-1} for samples from solvothermal synthesis and 1461(50) m^2g^{-1} for samples from microwave synthesis were obtained. The BET surface area of MFU-2 examined in sorption cycles after catalysis became negligible (ca. 3 m^2g^{-1}). Theoretical values of the specific surface area derived from (idealised) crystal lattice models were obtained from a Monte Carlo integration technique, in which a probe molecule was "rolled" over the internal crystal surface.[48] Values obtained for a probe 3.686 Å in diameter were 4117 m^2g^{-1} for MFU-1 and 1447 m^2g^{-1} for MFU-2; the latter corresponding well with the average surface areas determined for MFU-2 (1467 m^2g^{-1}). The pore volumes were evaluated by using the Dubinin–Radushkevich (DR) equation and compared to the theoretical values obtained from the crystallographic data (by using PLATON/SQUEEZE). The obtained pore volumes were 0.57 $mL\,g^{-1}$ for MFU-1 obtained by solvothermal synthesis and 0.56 $mL\,g^{-1}$ for MFU-1 from microwave synthesis (expected: 1.49 $mL\,g^{-1}$), and 0.55 $mL\,g^{-1}$ for MFU-2 obtained by solvothermal synthesis and 0.53 $mL\,g^{-1}$ for MFU-2 from microwave synthesis (expected: 0.55 $mL\,g^{-1}$). The values of micropore surface areas and volumes for MFU-1 are still high, when compared to those of microporous zeolites and aluminophosphates, but significantly lower than theoretically predicted values, or the corresponding experimental values of MOF-5 and other structurally similar MOF compounds (600–3400 m^2g^{-1}).[50] The huge discrepancy between experimental and theoretical values of surface area and pore volume for MFU-1 might be attributed to the presence of partially filled sections within the real crystal structure of MFU-1. It could be speculated that a partial filling of voids with a structural identical framework (i.e., framework interpenetration) occurred. However, clear-cut evidence from crystallographic studies was hampered by the many structural factors by which the real structure of MFU-1 differed from its idealised model, as discussed in the previous section. In addition, recent studies on the related framework MOF-5 revealed a minor phase consisting of doubly interpenetrated MOF-5 networks. In this case, the presence of lattice interpenetration changed the symmetry from cubic to trigonal and explained the peak splitting observed in the powder XRD patterns, as well as the reduced surface areas and pore volumes.[51]

UV/Vis spectroscopy: UV/Vis spectra of both compounds are in complete agreement with the coordination environment revealed by X-ray single-crystal structure analysis (see the Supporting Information): each Co^{II} centre is placed in a distorted tetrahedral coordination environment consisting of four aromatic N donors stemming from pyrazolate ligands in the case of MFU-2, and three N donors and a single dianionic oxo ligand in the case of MFU-1. The UV/Vis diffuse reflectance spectra (see the Supporting Information) of both compounds showed several similar absorption bands in the UV region, which corresponded to intraligand $n\rightarrow\pi^*$ and $\pi\rightarrow\pi^*$ transitions (see the Supporting Information). In the visible region, MFU-1 had a broad absorption band centred at 610 nm (16393 cm^{-1}), which could be assigned to the spin-allowed d–d transition $^4A_2(F)\rightarrow{}^4T_2(P)$ of tetrahedral Co^{II} ions.[52] Additional spectroscopic features included a weak shoulder at 550 nm (18182 cm^{-1}), and an absorption band in the near-infrared (NIR) region at 1000 nm (10000 cm^{-1}) assigned to the $^4A_2(F)\rightarrow{}^4T_2(F)$ transition. A band present at 270 nm (37040 cm^{-1}) might be ascribed to a Co^{2+}–O^{2-} charge transfer.[40, 53] MFU-2 possessed broad absorption bands centred at 596 nm (16779 cm^{-1}) due to the $^4A_2(F)\rightarrow{}^4T_2(P)$ of tetrahedral Co^{II} ions and at >1100 nm (> 9100 cm^{-1}) for the $^4A_2(F)\rightarrow{}^4T_2(F)$ transition. The observed spectral features for both MFU-1 and MFU-2 correspond well with literature values of tetrahedral Co^{II} complexes.[52]

After catalysis employing *tert*-butyl hydroperoxide, an additional, intensive band appeared at 410 nm (24390 cm^{-1}) in the UV/Vis spectrum of MFU-1. This single absorption band was characteristic of tetrahedral Co^{III} complexes,[40] and had been previously attributed to a ligand-to-metal charge-transfer transition[53a] from an oxygen atom to Co^{III}. A tetrahedral coordination environment is rarely observed for cobalt(III) atoms and is found, for instance, in the case of dodecatungstate as tetrahedral ligand[53a] or for a cobalt(III) imido complex with a scorpionate (=hydrotris(pyrazol-

1-yl)borato) ligand.[54] On the contrary, the more common octahedral Co^{III} complexes show two bands with nearly identical intensity at 300–450 nm for the $^1A_{1g} \rightarrow {}^1T_{2g}$ transition and at 450–850 nm for the $^1A_{1g} \rightarrow {}^1T_{1g}$ transition.[52] In contrast, the electronic spectrum of MFU-2 examined after catalysis remained virtually unchanged under similar conditions.

Catalytic activity of MFU-2 employing *tert*-butyl hydroperoxide: The stability of a catalyst against hydrolytic decomposition is a necessary pre-condition for many oxidation processes, since water is often obtained as a side product. The hydrolytic stability of MFU-1 was already reported in a previous communication.[31] The stability of MFU-2 against hydrolysis was investigated by several experiments. First, crystals of MFU-2 were suspended in ethanol (employed as a test protic solvent) for 96 h, after which time no discernible changes occurred in the UV/Vis spectrum or the XRPD pattern (see the Supporting Information). This characteristic remained unaffected when increasing amounts of H_2O were added to the crystal suspension (up to 30 vol% H_2O). In long-term experiments we could not find any signs of degradation when MFU-2 crystals were stored under ambient conditions (>6 months), which was in sharp contrast to the moisture sensitivity of many zinc terephthalate type MOFs.

To compare catalytic activities of both frameworks, our previous report about the liquid-phase oxidation of cyclohexene by *tert*-butyl hydroperoxide in the presence of MFU-1[31] was complemented by similar investigations conducted for MFU-2, which are described in the following section. For MFU-1, we showed that the heterogeneous catalytic reaction took place inside the pores of the MOF lattice.[31] X-ray powder diffraction data for the recovered catalyst gave no signs of framework decomposition. During reaction with *tert*-butyl hydroperoxide, microcrystals of MFU-1 underwent a slow colour change from blue to green and the BET surface of MFU-1 was found to become slightly reduced from 1485 to 1018 m^2g^{-1} after the first catalytic run.

The experimental data for the liquid-phase oxidation of cyclohexene by MFU-2, employing *tert*-butyl hydroperoxide as the oxidant, demonstrated that oxidation of cyclohexene was fast and multiple turnover was achieved (Figure 16), similar to the results reported previously for MFU-1. Whereas the oxidation reaction that occurred in the absence of catalyst was almost negligible (ca. 1% conversion after 12 h), the maximum cyclohexene conversion after 22 h for MFU-2 was 16% (TON=27), and the main reaction products were *tert*-butyl-2-cyclohexenyl-1-peroxide, followed by 2-cyclohexen-1-one and cyclohexene oxide, as revealed by combined gas chromatographic and mass spectrometric product analysis. The conversion achieved by using MFU-2 was slightly lower than that of MFU-1 under the same experimental conditions (MFU-1: 27.5% cyclohexene conversion after 22 h, TON=27). The product distributions in both cases, however, were almost identical.

Despite the seemingly similar catalytic properties of both frameworks, MFU-2 showed marked differences when compared with MFU-1 after the reaction with *tert*-butyl hydroperoxide and cyclohexene. For MFU-2, no colour change was observed during catalysis. Though the crystal morphology was retained, the X-ray powder diffraction pattern of the recovered catalyst showed an amorphous product (Supporting Information). In accordance with this finding, BET analysis revealed a loss of porosity (drop from 1675 $m^2g^{-1}$to ca. 3 m^2g^{-1}). These changes for MFU-2 indicated decomposition of the catalyst in contrast to the characteristics of MFU-1, as exemplified in the following paragraphs.

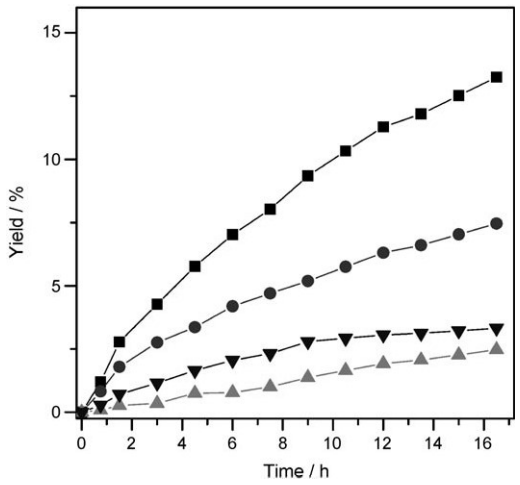

Figure 16. Yield [%] versus time [h] curves for cyclohexene oxidation with MFU-2 as the catalyst. Reaction conditions: cyclohexene (16 mmol), *t*BuOOH (8 mmol), 1,2,4-trichlorobenzene (2 mmol; internal standard), MFU-1 or MFU-2 (0.095 mmol based on cobalt centres), $T=70$°C. ■: total conversion, ●: *tert*-butyl-2-cyclohexenyl-1-peroxide, ▲: 2-cyclohexen-1-one, ▼: cyclohexene oxide.

Metal-leaching behaviour: To confirm the heterogeneous nature of the catalytic test reactions, we performed hot-filtration experiments, since it was known that even very small amounts of metal ions leaching into solution could be the single source of the observed catalytic activity with metal-substituted zeolite catalyst.[55]

Typical catalytic test runs were conducted as previously described. Upon reaching a substrate conversion of approximately 50% (which took about 2 h for MFU-1 and 4.5 h for MFU-2), the catalyst particles were removed from the hot solution by isothermal filtration. The filtrate obtained from the test run containing MFU-1 showed no significant catalytic conversion upon catalyst removal, indicating that contributions of soluble species towards catalytic activity were negligible (Figure 17). In contrast to this, the filtrate from a reaction mixture containing MFU-2 shows only a slightly diminished catalytic activity, as can be seen in Figure 17. The different behaviour of both MOFs in hot filtration experiments indicates that MFU-1 behaves as a truly heterogeneous catalyst, whereas the catalytic activity of MFU-2 is mostly due to soluble metal complexes leaching from the framework under catalytic conditions. This conclusion has support from complementary structural investigations, which

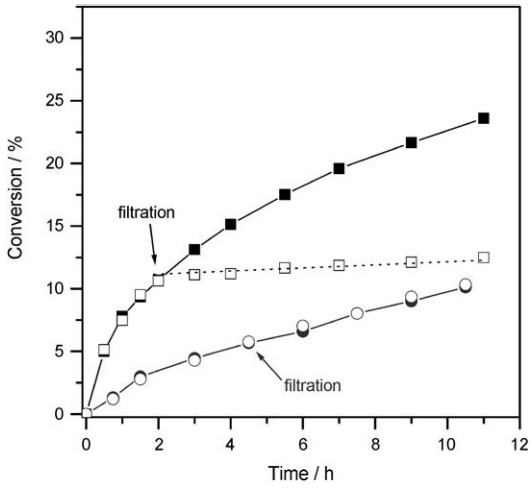

Figure 17. Conversion [%] versus time [h] curves for cyclohexene oxidation with MFU-1 (■) or MFU-2 (●) as the catalyst and after removing the catalyst from suspension after 2 (□) or 4.5 h (○).

demonstrate a loss of porosity and crystallinity for MFU-2 samples under catalytic conditions.

All filtrates from experiments described above were additionally analysed by atomic absorption spectroscopy (AAS). These studies yielded a surprising result: the amount of "free" Co^{II} ions in the filtrate was below 1.1×10^{-3}% for both test series (and thus beyond the lower detection limit of the AAS instrument.). Whereas for MFU-1 this finding is in accordance with the heterogeneous nature of the catalyst, the unexpectedly low concentration of cobalt ions in the case of MFU-2 indicates that the homogenously dissolved species liberated from MFU-2 possess a high catalytic activity.

Additional AAS experiments indicated that leaching of Co species from the MOFs was accelerated with an increasing amount of *tert*-butyl hydroperoxide. In the absence of cyclohexene, both frameworks decompose quickly, leading to a nearly quantitative release of soluble Co ions into the solution. Leaching can be vastly reduced by increasing the amount of cyclohexene, which indicates that the equilibrium between cobalt ions coordinated to the solid frameworks and those forming soluble species, is shifted in favour of the MOFs by a careful adjustment of the cyclohexene/*tert*-butyl hydroperoxide ratio (Table 4). Apart from this, the reaction temperature plays a crucial role in leaching behaviour: At 80 °C, the catalytic activity of MFU-1 increases remarkably, but in this case slight metal leaching is observed in hot-filtration experiments.

Table 4. Concentrations of cobalt ions determined by AAS (after a reaction time of 24 h).[a]

Ratio *t*BuOOH/cyclohexene	Leached Co ions [%]	
	MFU-1	MFU-2
1:0	50.12	52.30
3:1	0.011	0.004
1:1 or 1:2	<0.001	<0.001

[a] Reaction conditions: cyclohexene (0, 2.7, 8 or 16 mmol, as indicated), *t*BuOOH (8 mmol), 1,2,4-trichlorobenzene (2 mmol) (as an internal standard), MFU-1 or MFU-2 (0.095 mmol based on cobalt centres), T= 70 °C.

X-ray absorption spectroscopic investigations: To investigate structural changes of the coordination and the redox states of the cobalt centres of the MOFs before and after catalysis, extended X-ray absorption fine structure (EXAFS) and X-ray absorption near-edge structure (XANES) measurements were performed at the cobalt K edge. Possible changes (if any) in the catalytic centres (MOF nodes) could be undetected by XRD measurements if no long-range crystallographic order was present and might have been characterised by EXAFS and XANES measurements as well.

In EXAFS, an electron is displaced from its shell (or completely from the absorbing atom) and interacts with its neighbouring atoms. Depending on the wavelength (energy) of the electron and the interatomic distances, constructive or destructive interference of the electron waves can occur, thus EXAFS provides information about the local atomic environment around the absorbing atom. Close to the edge energy of the absorbing atom, valence-shell electron transitions have to be considered, and thus the information from XANES spectroscopy is complementary to UV/Vis spectroscopy, since the observed features are due to valence-shell electron transitions and are thus influenced by the number, coordination geometry and chemical nature of the surrounding ligands.

Each measurement was repeated at least three times and the average of the measured data was taken. The Co K-edge EXAFS spectra were analysed by using the standard Athena and Artemis FEFF XAFS analysis codes,[56] fitting to models derived from the single-crystal structure data. The fitted parameters (path lengths, Debye–Waller factors and energy shifts) are given in the Supporting Information. The raw and fitted Fourier transforms of the k^3-weighted $\chi(k)$ spectra at the Co K edge are shown in Figure 18, and the obtained atomic distances before and after catalysis are given in Table 5 and compared with the values from the crystal structure analyses. A comparison of the XANES spectra of MFU-1 before and after catalysis is given in Figure 19 below, indicating only a slight increase in the average oxidation state after catalysis.

For MFU-1, differences are discernible for the EXAFS spectra before and after catalysis (Figure 18): While the main features are retained, slight differences in the Fourier-transformed spectrum above 2 Å can be seen. The region from 0 to 2 Å corresponds to the first coordination shell and is, within statistical accuracy, identical in both cases, revealing that the fourfold coordination of Co atoms remains unchanged.

To derive a model for the changes in the $[Co_4O(3,5\text{-dmpz})_6]$ coordination unit of MFU-1 upon catalysis, different structures were tested, of which the model displayed in Figure 18 still gave the best fit. Differences between both EXAFS fitting curves shown in Figure 18 are thus expressed in terms of slightly changing distances and Debye–Waller

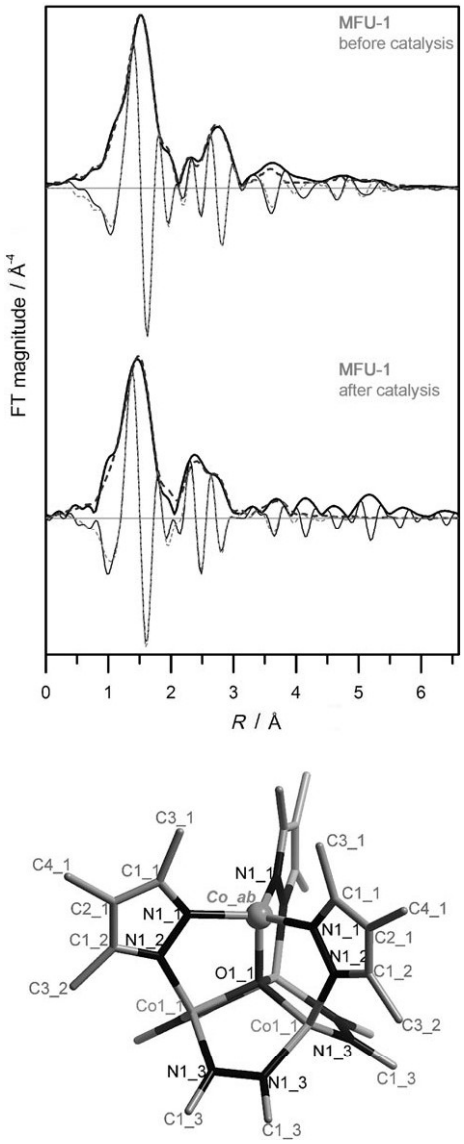

Figure 18. Top: Magnitude (bold line) and imaginary part (thin line) of the k^3-weighted Fourier transformation versus the radial distance R from the absorbing atom of the EXAFS spectra of MFU-1 before catalysis (top, k range = 1–12, fitted from 1.0–5.0 Å with 17 variables for 27 independent points, $R = 0.0004$ and reduced $\chi^2 = 82$) and after catalysis (bottom, k range = 1–14, fitted from 1.0–5.0 Å with 15 variables for 33 independent points, $R = 0.0026$ and reduced $\chi^2 = 90$). The raw data and the fitting curve are shown as solid and dashed lines, respectively. Bottom: Stick representation and labelling of the cluster used for EXAFS data analysis. The absorbing Co atom is highlighted as a filled sphere.

factors. Alternative structural models incorporating additional oxygen atoms coordinated to the Co centres gave higher R and χ^2 values (poorer fits) and gave unreasonably huge shifts for some distances (in particular, for the Co···Co distances).

Literature values of Co–O distances for cobalt ions in tetrahedral coordination sites are 1.93(6) Å for cobalt(II) and 1.81(3) Å for cobalt(III).[27, 57] For MFU-1 after catalysis, the Co–O distance is 1.87(1) Å, according to the EXAFS fitting data, which is lower than the original value (2.00(3) Å) before catalysis (Table 5), but is still in a value range in favour of a cobalt(II) centre in a tetrahedral coordination site. Moreover, the structural changes relating to the Co–N distances are negligible. Two scenarios are possible: either only negligible geometrical changes occur equally on all $\{Co_4O\}$ clusters or only a small fraction of the clusters in MFU-1 are changed during the course of catalysis.

Table 5. Half of the path length R as obtained by the fit to the EXAFS data, corresponding to the bond distance (for single-scattering contributions), for MFU-1 before and after catalysis, compared with the distances from single crystal X-ray structure analysis. The path labelling refers to the coordination unit shown in Figure 18.

Scattering path	Before catalysis [Å]	After catalysis [Å]	Crystal structure [Å]
Co_{ab}–O_{1_1}	2.00(3)	1.87(1)	1.95
Co_{ab}–N_{1_1}	1.97(1)	2.00(1)	1.98
Co_{ab}–N_{1_2}	2.88(2)	2.83(1)	2.88
Co_{ab}–C_{1_1}	3.07(2)	3.20(2)	3.07
Co_{ab}–Co_{1_1}	3.18(2)	3.15(3)	3.18
Co_{ab}–C_{3_1}	3.38(4)	3.38(3)	3.53
Co_{ab}–C_{1_2}	4.01(12)	4.04(5)	4.05
Co_{ab}–C_{2_1}	4.09(12)	4.12(5)	4.20
Co_{ab}-N_{1_1}-C_{2_1}-N_{1_1}	4.08(11)	4.19(4)	4.22
Co_{ab}–N_{1_3}	4.29(8)	4.23(2)	4.37
Co_{ab}–C_{3_2}	5.32(9)	5.13(4)	5.35
Co_{ab}–C_{4_1}	5.66(6)	5.38(4)	5.62
Co_{ab}–C_{1_3}	5.71(6)	5.42(4)	5.63

To complement EXAFS data for MFU-1, XANES spectra were examined, providing specific information about the valence state(s) of the cobalt ions in MFU-1 before and after catalysis. Figure 19 shows the XANES spectra of MFU-1 before and after catalysis. The shapes of both XANES spectra are very similar and it can therefore be concluded that the local coordination environments for the huge majority of cobalt centres are tetrahedral and thus identical. The most significant features of the XANES spectra are charac-

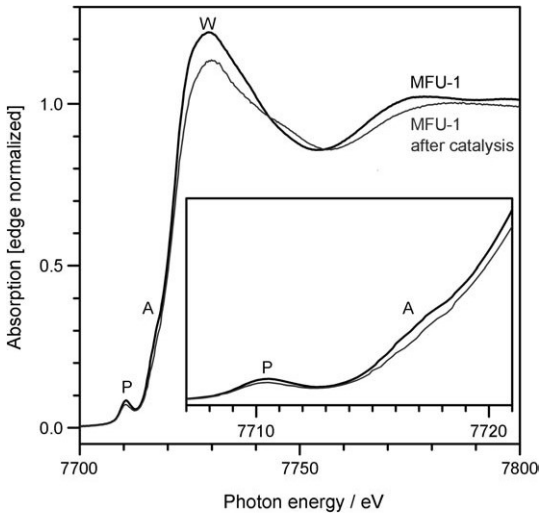

Figure 19. Normalised Co K-edge XANES spectra. P = pre-edge peak, A = peak edge; W = white line.

terised by the pre-edge peak (P in Figure 19), the absorption edge (A in Figure 19) and the white line (W in Figure 19).

The pre-edge structures at the Co K edges (P) usually fall into the energy range between 7709 and 7712 eV (here: 7710.5 eV) and can be ascribed to quadrupole 1s–3d and/or to modifications of dipole transition probability due to hybridisation between 3d and 4p states (since the dipole 1s–3d transition is dipole forbidden).[58] When the metal is located in a non-centrosymmetric site, such as in a tetrahedral complex, extensive molecular orbital mixing of the metal 3d orbitals with the metal 4p orbitals occurs, thus making the 1s to 3d–4p mixed orbital transition angular momentum allowed. This mixing is known to be more extensive in tetrahedral than in (pseudo)octahedral complexes and increases as the coordination number decreases. Perfectly octahedral (centrosymmetric) complexes are expected to have no pre-edge features in the XANES spectrum because both $A_{1g} \rightarrow T_{2g}$ and $A_{1g} \rightarrow E_g$ electronic transitions are Laporte forbidden.[59] Thus, for both MFU-1 samples, a non-centrosymmetric ligand environment around the cobalt ions is most probable. Comparing the samples before and after catalysis, the pre-edge peaks are nearly identical, and only a slight decrease in intensities occurs for the MFU-1 sample after catalysis. The first strong absorption (A) occurs as a shoulder on the low-energy side, as clearly indicated by a distinct peak in the first-derivative plots of all XANES spectra. Because of its high intensity, shoulder A must be assigned to a metal 1s to 4p transition; a dipole-allowed transition. In the absence of any "shake-down" contribution, the energy of shoulder A, and hence, the absorption edge energies (energies of the three metal 4p orbitals) are 7716.1 and 7716.5 eV before and after catalysis, respectively. A shift in the edge energies usually indicates a change in the oxidation state. The peak edge should be shifted to higher energy for cobalt centres of larger oxidation state; a systematic trend that is often utilised to estimate the oxidation state of cobalt,[60] whereby a linear dependence of the chemical shift on the average valence can be assumed.[61] Examination of reference samples (elemental cobalt, Co_3O_4 and Co^{III} pyrazolate)[62] also show this linear relationship (a shift of 3.69 eV per oxidation state occurs, see the Supporting Information for more information), from which an oxidation state of +2.08(7) can be extrapolated for MFU-1 after catalysis. As already seen from the two spectra in Figure 19, this change is quite small (too small to be accurately quantified), but discernible, providing further support for our previous statements according to which only a small fraction of $\{Co_4O\}$ units are affected after catalytic runs. Finally, a slight change in the coordination geometry around cobalt is also indicated by the decrease in the intensity of the white line (W) that shifts from 7729.4 to 7729.9 eV. These findings from XANES are in agreement with the changes observed in the bond lengths (EXAFS) and the results from UV/Vis. In conclusion, the most likely explanation for the observed spectral and structural changes occurring in MFU-1 upon catalysis is that just a small fraction of cobalt centres/coordination units is affected by the catalytic reaction conditions, for which a change in the valence state from (II) to (III) seems most likely. The presence of cobalt(III) centres is corroborated by UV/Vis and XPS[31] experiments, the exact amount of which is below a concentration level that would allow a more quantitative determination and thus preventing us from making a detailed structural characterisation of the cobalt species that appear under catalytic conditions.

Whereas EXAFS curves of MFU-1 show clear differences in samples before and after catalysis (especially above 2 Å in the Fourier-transformed spectra), the coordination environments and valence states of the cobalt ions in MFU-2 are completely preserved under catalytic conditions (see the Supporting Information). Since XRPD investigations reveal a loss of crystallinity and porosity for this framework under catalytic conditions, the results from X-ray absorption spectroscopy (XAS) investigations appear surprising at first glance. However, according to AAS investigations under catalytic conditions, only a tiny amount of soluble cobalt species leaches into solution, which might be explained by a collapse of the porous framework due to the removed cobalt ions, composed of MFU-2-like fragments.

The excellent fits to the EXAFS data for both MFU-1 and MFU-2 for the samples before catalysis support the validity of the structure obtained from single-crystal X-ray structure analysis. In particular, no distinct cobalt-containing species are observable, suggesting that the catalytic activity is due to the metal sites in these two MOFs (and not due to further unknown cobalt-containing impurities or side products in the voids of the network). After employing MFU-1 in catalysis, slight changes in the EXAFS and XANES spectra are observed.

When summarising results from spectroscopic and structural investigations obtained so far, the following interpretation seems permissible in light of catalytic properties: although tetrahedrally coordinated cobalt(II) centres are present in both frameworks, their metal centres are remarkably resistant against oxidation (yielding cobalt(III)) and they show no tendency to accept further ligands in their first coordination spheres. The stabilisation of the cobalt(II) oxidation state seems to be an intrinsic property of these frameworks. Usually, cobalt(III) peroxo complexes of, for example, *N*,*N*′-ethylenebis(salicylimine) (salen) or porphyrin complexes are kinetically inert due to their low-spin d^6 configuration, thus a large number of such complexes have been isolated and characterised at room temperature.[63] However, due to steric hindrance and constraints upon the possible distortion of individual coordination environments of the cobalt centres by the 3D network, coordination of an additional ligand would constitute an energetically unfavourable situation, and thus a strained or entatic state as described above. A similar stabilisation is also seen in structurally related tetrahedral cobalt of tridentate scorpionate ligands comprising bulky substituents at the pyrazolate moieties.[64] An octahedral coordination environment is also disfavoured for these complexes due to steric reasons and complexes with peroxides or oxygen can be only isolated in rare cases[64a] at low temperatures (< -50 °C for peroxo complexes

and <-10 to 30 °C for dioxygen complexes), and the reactive intermediates usually oxidise the pyrazolate ligands in a subsequent reaction at higher temperatures.

Principally, diffusion limitation might be another reason why only a minor part of the metal centres participates to the oxidation process.[65] However, in case of oxidation reactions involving *tert*-butyl hydroperoxide and cyclohexene, previous experiments employing microcrystals of different sizes showed that diffusion limitation was present to some extent, but it did not exert a major influence on the experimental reaction rates in MFU-1.[31]

Mechanism of *tert*-butyl hydroperoxide activation: The fact that *tert*-butyl-2-cyclohexenyl-1-peroxide is the main reaction product suggests a reaction pathway in which freely diffusing peroxy radicals are generated by cleavage of *tert*-butyl hydroperoxide following the route of a Haber–Weiss-type decomposition at the Co^{II} metal centres (Scheme 1).[63c, 66] The net reaction equation can be formulated as Equation (3):

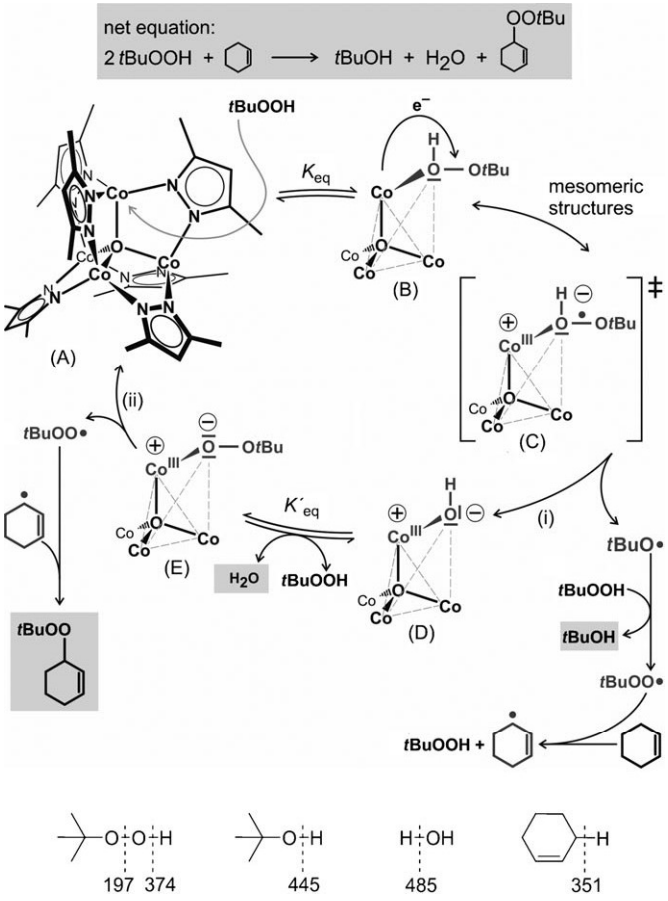

Scheme 1. Top: Mechanism for the formation of *tert*-butylperoxy radicals catalysed by the cobalt(II) centres in MFU-1. Their further reaction with cyclohexene, forming the main product, is shown. Bottom: Homolytic O–H and C–H bond dissociation energies [kJ mol^{-1}][63c, 66] of the educts, products and intermediates involved in the catalytic formation of *tert*-butylperoxy radicals by MFU-1.

$$3\,(CH_3)_3COOH \rightarrow 2\,(CH_3)_3COO^{\bullet} + (CH_3)_3COH + H_2O \quad (3)$$

A further hint toward a reaction path involving free radicals is given when the oxidation reaction is performed in CH_2Cl_2, as opposed to the solvent-free method that is generally applied. In this case, 3-chlorocyclohexene appears as an additional byproduct. Moreover, radical trap experiments confirm the formation of *tert*-butyl peroxy radicals and cyclohexenyl radicals throughout the course of the catalytic reaction (see the Supporting Information). In consideration of the homolytic bond dissociation energies of the involved substrates and products,[67] a detailed catalytic cycle (in analogy to earlier reports for similar reactions)[63c, 66] for the formation of *tert*-butyl peroxy radicals catalysed by MFU-1 can be proposed (Scheme 1).

In the first step, *tert*-butyl hydroperoxide is expected to coordinate to the cobalt centres in MFU-1 (Scheme 1, K_{eq}). Thermodynamic considerations suggest that the weak O–O bond of *tert*-butyl hydroperoxide (rather than the considerably stronger O–H bond) is cleaved by the aid of the Co^{II} ions in MFU-1 (Scheme 1(i)). Thus, *tert*-butoxy radicals and hydroxyl radicals might be created.[67] The resulting *tert*-butoxy radical might exchange a hydrogen atom with another *tert*-butyl hydroperoxide molecule ($\Delta H \approx -71$ kJ mol^{-1} from the bond dissociation energies) in a fast subsequent reaction ($k = 1.3 \times 10^8$ M^{-1} s^{-1} for the comparable reaction of cumyloxy radicals with *tert*-butyl hydroperoxide).[68] Consequently, a *tert*-butyl hydroperoxy radical and *tert*-butanol would be created. A minor fraction of the *tert*-butoxy radicals might also react directly with cyclohexene to yield a 3-cyclohexenyl radical ($k = 5.7 \times 10^6$ M^{-1} s^{-1}).[69] The hydroxy radicals created in the first step, or hydroxy anions if electron transfer occurs from Co^{II}, most likely react with another *tert*-butyl hydroperoxide molecule under formation of water (Scheme 1, K'_{eq}). The resulting cobalt hydroperoxo species could react further through fission of either the O–O or the Co–O bond. However, the coordinative bonds between the peroxo ligands and the Co^{III} centres are probably very weak, owing to the steric shielding of the metal ions and the rigid coordination geometry imposed by the crystalline framework. This assumption is supported by the low isosteric heat of adsorption of molecular oxygen and the unchanged IR spectra after a catalytic run employing *tert*-butyl hydroperoxide (see the Supporting Information). This special situation presumably leads to formation of *tert*-butyl peroxy radicals (by fission of the cobalt–oxygen bond (as proposed in Scheme 1(ii)) rather than to homolytic fission of the oxygen–oxygen bond of the coordinated peroxo ligand. After recovering the initial catalyst by removing the resulting *tert*-butyl hydroperoxy radical from the Co atom in the framework, the catalytic cycle starts over again. In a subsequent step, the formed *tert*-butylperoxy radicals would react with cyclohexene to yield the observed products (Schemes 1 and 2). Two pathways are possible for the subsequent reaction of *tert*-butyl peroxy radicals with cyclohexene. First, the abstraction of a hydrogen atom from the allylic position of

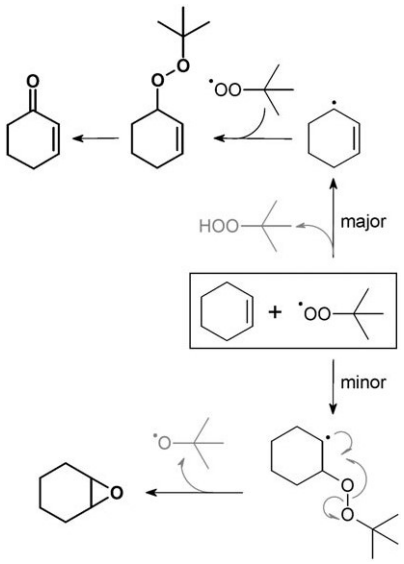

Scheme 2. Formation of the observed products through the reaction of *tert*-butyl peroxy radicals with cyclohexene.

cyclohexene, and second the addition of the radical to the double bond. Whereas the second case is usually observed, for instance, in the case of carbon-centred radicals,[70] for *tert*-butyl peroxy radicals predominantly (≈98%) the abstraction of an allylic proton is observed.[71] Radical combination of the resulting 3-cyclohexenyl radicals with another *tert*-butyl peroxy radical would yield the observed main product, *tert*-butyl-2-cyclohexenyl-1-peroxide. The byproduct 2-cyclohexen-1-one is most likely formed by thermal decomposition of the main product.[72] The addition of *tert*-butyl peroxy radicals to the double bond as a minor reaction followed by cleavage of a *tert*-butoxy radical should lead to cyclohexene oxide, which explains the formation of the other byproduct observed.

Only the asymmetric product of the radical recombination between *tert*-butyl peroxy and 3-cyclohexenyl radicals is found. No symmetric product, for example, 3,3′-bicyclohexene, can be observed from the recombination of two 3-cyclohexenyl radicals. Such a preference of the asymmetric product in radical recombination reactions can be explained by the Ingold–Fischer "persistent radical effect".[73] Cross-coupling occurs when one radical is "transient" (undergoing fast reactions) and the other is "persistent" (longevity by, for example, steric crowding), and both are generated at comparable reaction rates. Thus, a steady state involving high concentrations of persistent and low concentrations of transient radicals occurs, leading to preferred cross-coupling. The Ingold–Fischer persistent radical effect was observed earlier for the homogenously catalysed and uncatalysed reactions between persistent *tert*-butyl peroxy radicals and transient cyclohexene radicals.[66d]

The fact that no substantial change in the IR, XANES or EXAFS spectra is observed after multiple turnovers indicates that the Co^{III} species are energetically unfavourable intermediates, which thus occur only in small concentrations and tend to decompose (recovering the initial Co^{II} species of the catalyst, whilst liberating the peroxy radicals).

Mechanism of O_2 activation: Due to its triplet electronic ground state, the spontaneous oxidation of organic substrates by molecular oxygen is often kinetically unfavourable, since its direct utilisation in reactions with singlet-state molecules is restricted by the Wigner spin conservation rule.[74] The diradical character of the free paramagnetic oxygen molecule thus leads to preferred reactions with radicals or paramagnetic metal ions.[75] The most numerous synthetic oxygen complexes are known for cobalt(II) compounds,[75] thus oxidation reactions employing MFU-1 should not only be possible when employing *tert*-butyl hydroperoxide as an oxidant, but also with molecular oxygen.

MFU-1 indeed shows a slow but constant reaction with molecular oxygen at $T > 120\,°C$, which is accompanied by a colour change from blue to green. A similar oxidation behaviour is not seen for MFU-2, which shows no sign of reaction with oxygen or decomposition below 230 °C. However, the interactions between O_2 and MFU-1 below 120 °C are weak, as expressed by an isosteric heat of adsorption of about only 11.1 kJ mol^{-1}, which is probably due to the effective steric shielding of the cobalt centres. The electronic interactions between dioxygen and cobalt centres in MFU-1 are clearly too weak to activate oxygen, since all attempts in our hands of gas-phase reactions between molecular oxygen and different hydrocarbons in the presence of MFU-1 have failed so far, showing no or extremely low yield of the anticipated products.[76]

In recent years, *N*-hydroxyphthalimide (NHPI, Scheme 3) has been recognised as a valuable co-catalyst (acting as an electron-transfer mediator) for the aerobic oxidation of organic compounds under mild conditions. The use of coupled catalytic systems with electron-transfer mediators usually facilitates the procedures by transporting the electrons from the catalyst to the oxidant along a low-energy pathway, thereby increasing the efficiency of the oxidation and thus complementing direct oxidation reactions. As a result of similarities with biological systems, this can be dubbed a biomimetic approach.[77] NHPI, as a co-catalyst, is transferred in combination with transition-metal complexes[78,81] into PINO by molecular oxygen (Scheme 3). NHPI is regenerated by abstracting a hydrogen atom from the substrate. In the case of MFU-1, a putative mechanism includes the chemisorption and activation of molecular oxygen by one of the cobalt(II) centres (Scheme 3, K_{eq}). In a subsequent step, the activated oxygen may abstract a hydrogen atom from NHPI (Scheme 3, K'_{eq}). Co–O bond fission would then recover the catalyst.

Another advantage of the reaction cascade employing PINO radicals is their higher reactivity than that of peroxy or oxy radicals. Since O–H bond dissociation energies for both NHPI and *tert*-butyl hydroperoxide are almost identical (≈370 kJ mol^{-1}),[79] the increased reactivity has to thus be explained by a "polar effect". The presence of two carbonyl groups is responsible for a pronounced electrophilic charac-

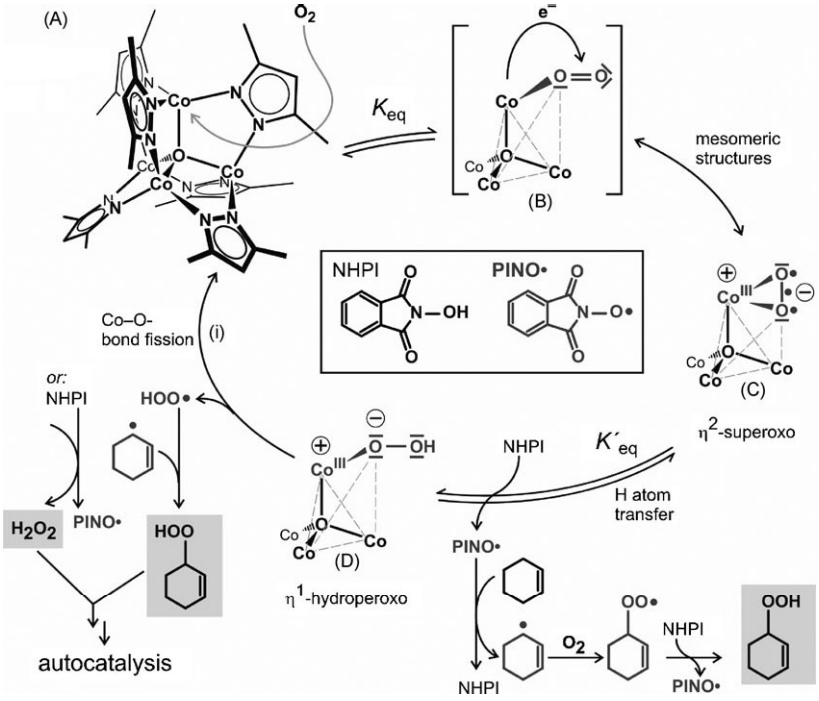

Scheme 3. Formation of phthalimide-*N*-oxyl radicals (PINO) from *N*-hydroxyphthalimide (NHPI) involving cobalt(II) centres.

ter of PINO, lowering the energy of the transition state (Scheme 4) and thus increasing its reactivity.[80]

MFU-1 (1 mol%) was capable of catalysing the oxidation of cyclohexene, ethylbenzene or cyclohexanol by using atmospheric oxygen at close to ambient conditions (i.e., 35°C, Table 6) when NHPI (10 mol%) was added. No conversion was observed in the absence of either components (MFU-1 or NHPI). Due to the poor solubility of NHPI in most organic solvents, the catalytic test reactions were carried out in acetonitrile.[81]

Under mild reaction conditions, cyclohexanol (Table 6, entry 1) was nearly completely transformed to cyclohexanone after 24 h, whereas secondary allylic or benzylic substrates were converted to peroxides or ketones, respectively (Table 6, entries 3–5). Higher temperatures facilitated the further decomposition of the peroxides (compare entries 4 and 5, Table 6). Non-activated C–H bonds, such as those from cyclohexane (Table 6, entry 2), showed only sluggish reaction even at elevated temperatures (yielding 1.5% cyclohexanone after 24 h). The observed reactivities were qualitatively in agreement with the expected behaviour for oxidation reactions performed by the NHPI/PINO system. The second-order rate constants for the hydrogen abstraction from different substrates by PINO (expressed per active hydrogen atom) at 25°C in acetonitrile were[81b] $k = 5.05\,\mathrm{M^{-1}s^{-1}}$ for cyclohexene, $k = 4.52\,\mathrm{M^{-1}s^{-1}}$ for cyclohexanol, $k = 1.12\,\mathrm{M^{-1}s^{-1}}$ for ethylbenzene and $k = 0.0039\,\mathrm{M^{-1}s^{-1}}$ for cyclohexane, thus the obtained reactivities in our experiments were explained. When monitoring the time course of the oxidation reaction of cyclohexene in detail (Table 6, entry 3), further mechanistic insights became apparent. During the first 8 h of the reaction, only low conversions

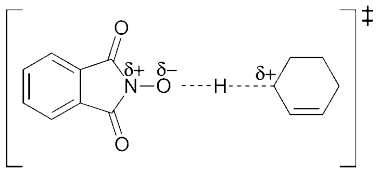

Scheme 4. Transition state for the reaction of PINO with cyclohexene.[81]

Table 6. Oxidation of hydrocarbons by molecular oxygen catalysed by MFU-1 and NHPI for 24 h.[a]

Entry	T [°C]	Educt	Products and yields [%]							Conversion [%]
1	35	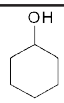	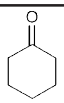	94						95
2	75			1.5						2
3	35			26.6	+		5.6	+	 0.8	35
4	35			5.1	+		1.2			7
5	45			1.7	+		14.5			18

[a] Reaction conditions (if not stated otherwise): atmospheric oxygen, NHPI (50 mg, 0.31 mmol), MFU-1 (15 mg, 0.038 mmol based on cobalt centres), 1,2,4-trichlorobenzene (150 µL, 1.2 mmol; internal standard), educt (3.0 mmol; cyclohexene (300 µL), ethylbenzene (365 µL), cyclohexanol (270 mg) or cyclohexane (300 µL)), acetonitrile (5 mL), $T = 35$°C, 24 h. The peroxides were identified by quantitative reduction to the corresponding alcohols by using triphenylphosphine and identified by their changed retention time in GC-MS.[82]

were observed (yielding ≈0.5% of 3-cyclohexenylperoxide), whereas after this induction period, the conversion rate increased rapidly (Figure 20). When the solid catalyst was filtered off from the reaction mixture after 16 h, the filtrate showed a drastically decreased catalytic activity, thus demonstrating that the reaction was heterogeneous in nature in this case as well. The remaining reactivity of the filtrate might be due to the spontaneous (non-catalysed) decomposition of 2-cyclohexenylperoxide and its reaction with NHPI. After a reaction time of 16 h, the MFU-1 catalyst did not change according to XRPD and IR analysis, and UV/Vis spectra indicated once again the partial formation of cobalt(III) for this reaction. However, long reaction times (greater than 32 h) exerted a detrimental effect upon the catalyst, which slowly decomposed to form an amorphous product. The decomposition of the framework in the presence of PINO was probably accelerated by the products developed during the reaction, in particular, due to the formation of a huge excess of 3-cyclohexenylperoxide.

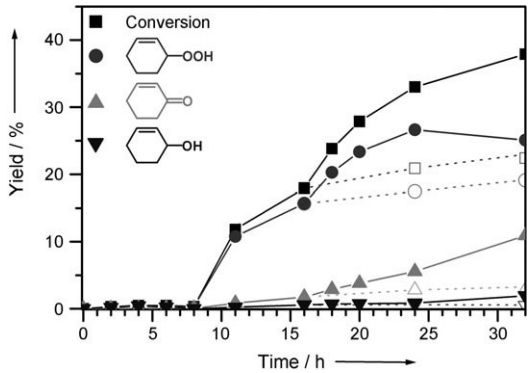

Figure 20. Conversion [%] and yields [%] for the reaction of cyclohexene and oxygen at 35 °C in the presence of catalytic amounts of NHPI and MFU-1 versus time. The dotted lines and empty symbols represent the time course of the reaction upon removal of the MFU-1 catalyst by filtration after 16 h.

The reason for the initial inhibition observed in the catalysis reaction was presumably due to autocatalysis of the reaction by the formed 2-cyclohexenylperoxide (see Scheme 3). Whereas initially the reaction was driven by the (slow) activation of oxygen on MFU-1 [Eqs. (4)–(7)], later on 2-cyclohexenyloxo and -peroxo radicals were formed during the course of the reaction, which appeared to be activated much faster at the cobalt(II) centres of MFU-1 [Eqs. (8)–(10)]. Accordingly, when catalytic amounts of *tert*-butyl hydroperoxide (1 mol%) were added at the beginning of the reaction, no inhibition was observed, yielding 19% of 2-cyclohexenylperoxide after 3 h. This appears to be due to efficient activation of peroxides by MFU-1, when directly compared with the corresponding activation of molecular oxygen. During the course of the reaction, the peroxy radicals should thus be mainly in charge of hydrogen abstraction from NHPI. A similar participation of peroxides is also seen in autoxidation reactions of cyclohexene or cyclopentene catalysed by rhodium, iridium or platinum complexes.[83]

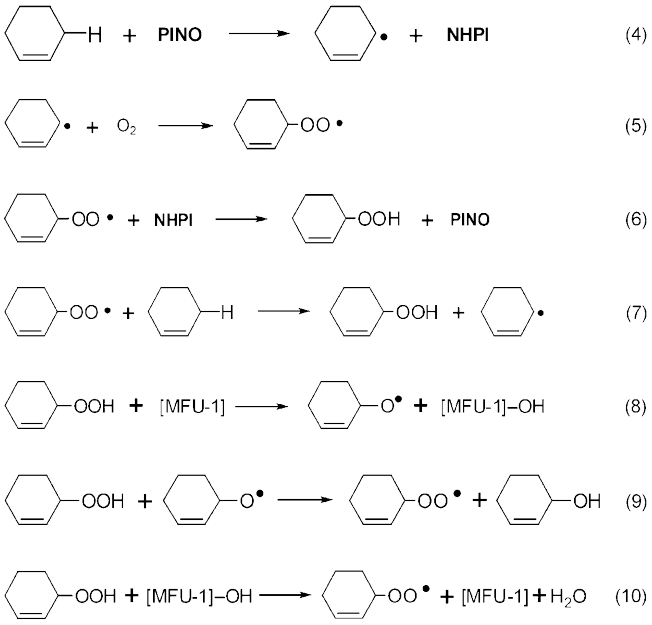

According to Equations (4) to (6), the PINO radicals abstract a hydrogen atom from cyclohexene, which subsequently reacts with molecular oxygen to yield 2-cyclohexenylperoxide. The net reaction is thus formulated according to Equations (4)–(10). Whereas at the initial stage of the catalytic reaction, PINO radicals are predominantly obtained from the reaction of NHPI with molecular oxygen (activated by cobalt centres), the former radicals are produced more efficiently at a later stage by catalytic decomposition of the reaction product 2-cyclohexenylperoxide.

Heterogeneous catalytic oxidation by using NHPI@MFU-1 and molecular oxygen: The advantage of heterogeneous catalysts lies in the ease of their recovery from reaction mixtures, allowing the reaction products to be obtained without additional purification steps. Additionally, the uniform pores of MFU-1 provide a means of size- or shape-selective catalytic oxidation reactions. These technical advantages are lessened by the use of a solution of NHPI in acetonitrile, due to the high costs of the solvent and the continuous loss of the co-catalyst upon filtration. Consequently, the immobilisation of both catalytic compounds, cobalt(II) and NHPI, would be preferable. This approach was successful for cobalt(II) salen complexes and NHPI derivates; both were covalently bound to a mesoporous silica carrier.[84] To immobilise NHPI in the pores of MFU-1, MFU-1 (15 mg) were suspended for 3 d in a solution of NHPI (50 mg) in acetonitrile (5 mL) (the same stochiometry as in the catalysis reactions described above). Afterwards, the MFU-1 material hosting the co-catalyst (termed hereafter NHPI@MFU-1) was filtered off and dried in vacuo. Indeed, NHPI@MFU-1 cata-

lysed the oxidation of cyclohexene at 35 °C without any additional solvent (Figure 21, filled symbols and solid lines).[85] Moreover, the activity of this heterogeneous system was

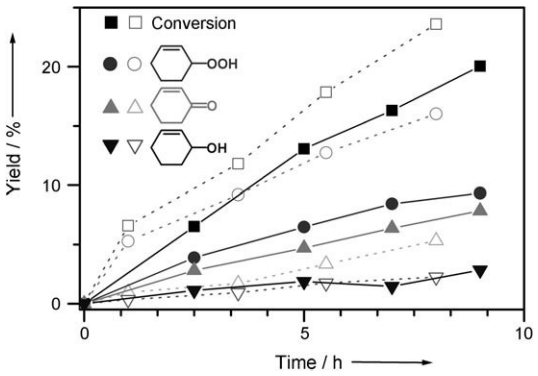

Figure 21. Conversions [%] and yields [%] versus time for the reaction of cyclohexene with molecular oxygen at 35 °C. Filled symbols and solid lines: solvent-free catalysis employing NHPI@MFU-1; Open symbols and dotted lines: catalysis employing MFU-1 suspended in NHPI-containing acetonitrile.

only slightly reduced in comparison with the system containing a homogeneous solution of NHPI in acetonitrile (Figure 21, open symbols and dotted lines).

Thus, the oxidation of cyclohexene (and presumably a huge range of other organic substrates) can be carried out as a suspension of NHPI@MFU-1 in the organic substrate, thus avoiding the use of additional solvent, simplifying workup procedures and reducing the amount of waste. Compared with the usually drastic conditions employed for the oxidation of cyclohexene (high oxygen pressure and high temperatures),[81a,86] the reaction can be carried out by using NHPI@MFU-1 under more cost-saving and environmental-friendly conditions (35 °C, atmospheric oxygen).

Conclusion

We have presented the solid-state structures of two pyrazolate-based MOFs (MFU-1 and MFU-2) of cobalt(II) centres connected by the linear linker 1,4-bis[(3,5-dimethyl)pyrazol-4-yl]benzene, which can be regarded as an N-heterocyclic derivative of terephthalic acid. MFU-1 constitutes a structural analogue of the Zn-containing (redox inactive) MOF-5, featuring oxo-centred tetranuclear $\{Co_4O\}$ cores, whereas MFU-2 is composed of cross-linked 1D cobalt(II) chains. The results from UV/Vis spectroscopy and XAS are in complete accordance with the structural data obtained from single-crystal X-ray analyses, demonstrating phase purity and the absence of other impurities containing cobalt(II). Both MOF compounds were compared in a catalytic test reaction by using cyclohexene as the substrate and *tert*-butyl hydroperoxide as the oxidant. Although Co^{II} are found in structurally similar (tetrahedral) coordination environments, contrasting metal-leaching behaviour is observed for both compounds under catalytic conditions: Whereas MFU-1 performs as truly heterogeneous and robust catalyst, MFU-2 (albeit showing a similar catalytic activity) suffers from metal leaching into solution. This clearly demonstrates the importance of conducting metal-leaching tests in catalytic investigations. The ability of the networks to adsorb and activate molecular oxygen was examined by measuring the isosteric heat of adsorption and by TPO experiments, revealing a higher oxygen affinity of MFU-1 than MFU-2. DFT calculations show that a superoxo complex might form between the $\{Co_4O\}$ nodes in MFU-1 and molecular oxygen, which displays a hugely distorted coordination polyhedron for the Co^{II} atom involved in coordination, leading us to propose a geometrically and energetically strained catalytic intermediate, that is, an entatic state of the catalyst. However, the activation energy for the formation of this superoxo complex is high, since below 120 °C, complex formation cannot be observed for MFU-1. Once formed, and in the absence of any easily oxidisable substrate, this highly reactive entatic species leads to rapid oxidation of the framework in multiple subsequent steps. At temperatures below 120 °C, oxygen shows only weak interactions with the cobalt centre of MFU-1, and the resulting adsorbed O_2 species can be described as a van der Waals complex. Despite the low coordination number, the cobalt centres show no tendency to open up their coordination spheres, which can be explained in terms of the steric shielding of the cobalt centres by the methyl substituents of the coordinated pyrazolate moieties and by symmetry constraints imposed by the 3D periodic arrangement of the SBUs; the latter represents a different kind of strained (i.e., entatic) state of the catalyst. The low coordination ability of the cobalt centres represents a distinct advantage in catalytic oxidation reactions, since the formation of stable cobalt complexes with oxygen-centred ligands is thus avoided, which might otherwise constitute a "thermodynamic sink" and thus a potential dead end of a catalytic cycle.[75] Preventing formation of a coordinative bond between O_2 and cobalt centres leads to the observed low isosteric heats of adsorption ($(11.1 \pm 0.9)\,kJ\,mol^{-1}$ for MFU-1 and $(8.5 \pm 0.9)\,kJ\,mol^{-1}$ for MFU-2). Owing to the weak binding of O_2 at low temperatures, we were therefore not able to characterise any structurally well-defined intermediate species. By employing *tert*-butyl hydroperoxide as an oxidant, the $\{Co_4O\}$ core of MFU-1 showed small geometrical changes under catalytic conditions, which we ascribed to an increase in the oxidation state from cobalt(II) to cobalt(III) (based on data from XAS and UV/Vis investigations), involving, however, only a small fraction of the total metal centres. A summary of the most significant results is given in Table 7.

In terms of catalytic applications, the activation of molecular oxygen by MFU-1 becomes feasible by taking advantage of a co-catalyst (NHPI), which can be immobilised in the framework, leading to the composite catalyst NHPI@MFU-1. The immobilised NHPI serves as an electron-transfer mediator, and thus, heterogeneous oxidation reactions em-

Table 7. Summary of characteristic data for MFU-1 and MFU-2.

	Pore aperture	BET surface [m^2g^{-1}][a]			Pore volume	After catalysis			Isosteric heat of adsorption	Metal leaching	Decomposition temperature[c] [°C]		
	[Å]	before catalysis	theoretical	after catalysis	[cm^3g^{-1}][b]	VTXPRD	EXAFS	XANES: Co oxidation state	[$kJ\,mol^{-1}$]	in catalysis	TGA	VTXRPD	TPO
MFU-1	9.0	1485 (1525)	4117	1018	0.56 (1.49)	unchanged	slight geometrical changes	2.08(7)	−11.1	no	340	270	120
MFU-2	6.4	1477 (1675)	1447	3	0.53 (0.55)	amorphous	unchanged	2.00(7)	−8.5	yes	340	300	230

[a] For samples from microwave syntheses; values for samples from solvothermal syntheses in parentheses. Theoretical values obtained by the program developed by Düren et al.[48] [b] For samples from microwave syntheses; theoretically expected from PLATON/SQUEEZE in parentheses. [c] Variations are due to the different sensitivities and conditions used for the different methods. TGA gives the temperature at which the ligand is released in an inert nitrogen atmosphere, whereas VTXRPD gives the temperature of phase transitions of the sample in static air. The TPO measurements give significantly lower decomposition temperatures, since decomposition products are already registered at slow decomposition rates due to the higher sensitivity of the MS. In addition, the gas flow rate has an influence on the decomposition temperature. Under static conditions, the presence of oxygen leads to totally different decomposition temperatures in comparison to a flowing atmosphere. In TA and VTXRPD experiments, a decomposition product has to reach a certain proportion to be detected by these methods. Thus, TPO with MS is the most sensitive method for investigating even small decomposition processes.

ploying molecular oxygen can be performed at near-ambient conditions.

The pronounced differences in catalytic behaviour displayed by the structurally similar compounds MFU-1 and MFU-2 indicate that little is known about structure–reactivity relationships in redox-active MOFs in general. Future research may target the reactions leading to oxidative degradation of the frameworks, as well as the influence of the chemical nature of coordinate cobalt species at the external boundary of the MOF microcrystals. Finally, by employing refined and more sensitive spectroscopic techniques, the structural characterisation of reactive MOF intermediates might become feasible, serving as an information source for detailed theoretical studies.

Experimental Section

Experimental methods and equipment used for investigations: *tert*-Butyl hydroperoxide (70% H_2O solution) was dried over anhydrous $MgSO_4$. *tert*-Butyl-2-cyclohexenyl-1-peroxide[87] and cobalt(III) pyrazolate[62] were synthesised according to literature procedures. Other materials were obtained from commercial suppliers and used without further purification. Hydrothermal syntheses of the MOFs were carried out on a TH20 temperature-programmable heating block by HLC Biotec and microwave-assisted syntheses were performed by using a CEM, Discover S-Class microwave system. FTIR spectra were recorded of KBr pellets in the range 4000–100 cm^{-1} on a Bruker IFS FTIR spectrometer. Elemental analyses (C, H, N) were carried out on a Perkin–Elmer 2400 elemental analyzer. Thermogravimetric analysis (TGA) was performed with a TGA/SDTA851 Mettler Toledo analyzer in the temperature range 30–800 °C in a flow of nitrogen at a heating rate of 10 °C min^{-1}. Two powder X-ray diffraction methods were used to characterise MFU-1 and MFU-2. Variable-temperature X-ray powder diffraction (VTXRPD) patterns were measured by using a diffractometer equipped with an Anton Paar HTK 1200N heating chamber (θ-θ mode, $Cu_{K\alpha}$ radiation, $\lambda = 1.5406$ Å) under static air. X-ray powder diffraction data for phase analysis were collected on a PANalytical X'Pert PRO diffractometer (θ-θ mode, $Cu_{K\alpha}$ radiation, $\lambda = 1.5406$ Å). Powder diffraction patterns were scanned over the angular range $2\theta = 5.0$–$50.0°$ in steps of 0.0334°, measured for 250 s per step (for all samples except microwave-synthesised MFU-1 at 10 s per step). UV/Vis diffuse reflectance spectra (DRS) were recorded on an Analytik Jena Specord 50 UV/Vis spectrometer in the range 190–1100 nm. Argon gas sorption isotherms were measured with a Quantachrome Autosorb-I ASI-CP-8 instrument. Prior to measurements, the samples of CH_2Cl_2-exchanged MFU-1 and MFU-2 were heated at 150 °C for 30 h in high vacuum to remove the occluded solvent molecules. Argon sorption experiments were performed at 77 K in the range $1.00 \times 10^{-4} \leq p/p_0 \leq 1.00$. Gas chromatographic analyses were carried out with a Carlo Erba GC 8380 gas chromatographic instrument with a hydrogen flame ionization detector. GC-MS data were recorded on a Varian GC 3800-Varian Saturn 2000 MS instrument equipped with a WLD/ECD detector and a Chrompack column (CP-5842, 25 m long). EXAFS and XANES measurements were conducted at RT by using the double crystal monochromator (SiGe (111) graded crystals, $E/\Delta E = 4200$) at the beamline KMC-2 of the electron storage ring at the Berliner Elektronenspeicherring-Gesellschaft für Synchrotronstrahlung m.b.H. (BESSY II, Berlin, Germany).[88] The XANES and EXAFS spectra were recorded at the Co K edge; energy calibration was performed with cobalt metal foil. Measurements were performed in transmission mode by using ionisation chambers, additionally the fluorescence was recorded by using a fluorescence yield detector (Si-PIN photodiode). AAS was performed on a Perkin–Elmer 4100ZL Zeeman atomic absorption spectrometer. 30 µL aliquots of the sample solution were dispensed automatically into the atomizer. The standard additions method was used for calibration: wavelength: 242.5 nm, slit: 0.2 nm, pretreatment at 1400 °C for 30 s, atomization at 2500 °C for 4 s, modifier: $Mg(NO_3)_2$ (15 µg), diluent: 0.2% HNO_3, characteristic mass: 17.0 pg, sensitivity: 20.0 µg L^{-1}, LOD calculated to 3 µg L^{-1}. Isosteric heats of adsorption: oxygen adsorption isotherms were recorded in a magnetic suspension balance (Rubotherm, Germany)[89] that could be operated up to 50 MPa. A scheme of the balance, including temperature and pressure sensors, and various gas supplies is shown in Figure S1 in the Supporting Information. Two different pressure transducers (Newport Omega, US) were used in a range from vacuum up to 5 MPa with an accuracy of 0.05%. In a typical experiment, a stainless-steel sample holder was filled with about 0.1–0.2 g of MFU-1 or MFU-2, respectively. The balance was evacuated for 12 h at 573 K and 0.3 Pa until constant mass was achieved. For measuring the sorption capacity, the gas was dosed into the balance chamber to elevated pressures. Equilibrium was achieved within 2 h, which is characterised by constant weight and pressure over a time range of approximately 15 min. The temperature was kept constant with an accuracy of ±0.1 K for each measurement. Additionally, for each isotherm, a buoyancy correction was used to calculate the surface excess mass from the measured values. A detailed description of this procedure can be found elsewhere.[90] For the determination of the density of oxygen from pressure and temperature, the program FLUID-

CAL was used.[91] Temperature programmed oxidation (TPO) and pulse chemisorption were performed on a Rubotherm/Bel Japan, BELCAT-B, instrument equipped with a quadrupolar mass spectrometer with a thermal conductivity detector (TCD) sensor. The TPO experiments were carried out in the temperature range up to 250 °C for MFU-1 and 300 °C for MFU-2 in 1000 ppm O_2 in He. All experiments were monitored with a quadrupolar mass spectrometer (GAM 400, InProcessInstruments, Germany).

Solvothermal synthesis of MFU-1: H_2-bdpb (10 mg, 0.037 mmol) was dissolved in hot (100–120 °C) DMF (4 mL) with the aid of an ultrasonic bath. After cooling to RT, $CoCl_2 \cdot 6H_2O$ (40 mg, 0.168 mmol) was dissolved in the resulting solution and a 1 M aqueous solution of HCl (0.01 mL, 0.01 mmol) was added. Then, the solution was placed in a heating tube (10 mL) that had been previously treated with a solution of $(CH_3)_2SiCl_2$ in chloroform (5% by weight). The heating tube was sealed and heated at a constant rate of 0.2 °C min^{-1} to 120 °C and kept at this temperature for 4 d. After hot filtration, MFU-1 was washed three times with DMF (20 mL), CH_2Cl_2 (10 mL), and suspended afterwards three times in CH_2Cl_2 (3 mL) for 24 h (followed by centrifugation and decantation each time), and was subsequently dried in vacuum for 6 h at RT prior to further investigations to yield blue cubic crystals of phase-pure MFU-1 (9.0 mg, 8.6 mmol, 70% based on ligand H_2-bdpb). IR (KBr): 3395 (br), 2924 (m), 2855 (w), 1679 (m), 1573 (m), 1493 (m), 1429 (s), 1374 (m), 1332 (m), 1286 (m), 1216 (w), 1108 (m), 1049 (s), 1013 (s), 981 (w), 846 (m), 754 (s), 665 (w), 617 (w), 582 (w), 524 (m), 490 cm^{-1} (s); elemental analysis calcd (%) for $Co_4O(C_{16}H_{16}N_4) \cdot 2(C_3H_7NO)$: C 54.44, H 5.25, N 16.47, found: C 51.60, H 5.87, N 16.10.

Bigger single crystals of MFU-1 that are more suitable for single-crystal X-ray structure analysis (edge lengths of 50–80 μm) were obtained when H_2-bdpb (15 mg, 0.056 mmol) was dissolved in hot DMF as described above and $Co(NO_3)_2 \cdot 6H_2O$ (100 mg, 0.34 mmol) was added to the solution when it had been cooled to RT. The solution then was heated immediately to 120 °C, at which temperature it was kept for 3 d. This procedure yielded MFU-1-enriched material, which was contaminated with MFU-2.

Microwave-assisted solvothermal synthesis of MFU-1: H_2-bdpb (96 mg, 0.36 mmol) was dissolved in hot DMF (16 mL, 100–120 °C) aided by an ultrasonic bath. After being cooled to RT, $Co(NO_3)_2 \cdot 6H_2O$ (138 mg, 0.47 mmol) was dissolved in the resulting solution and an aqueous solution of 1 M HCl (0.01 mL, 0.01 mmol) was added. Then, the solution was placed in a Pyrex sample tube (35 mL). The tube was sealed and heated for 2 min to 150 °C by employing a microwave synthesiser (CEM Discover S) at 300 W, after which time, phase-pure MFU-1 (113 mg, 0.11 mmol, 90% based on H_2-bdpb) was formed after being worked up as described above.

Solvothermal synthesis of MFU-2: H_2-bdpb (15 mg, 0.056 mmol) was dissolved in hot DMF (4 mL, 100–120 °C) aided by an ultrasonic bath. After being cooled to RT, $Co(NO_3)_2 \cdot 6H_2O$ (100 mg, 0.344 mmol) was added and dissolved, and the resulting solution was placed in a heating tube (10 mL). The heating tube was sealed and heated at a constant rate of 0.15 °C min^{-1} to 120 °C. After 10 h, the purple product was filtered when still hot and washed three times with DMF (20 mL) and CH_2Cl_2 (10 mL). Afterwards, MFU-2 was suspended three times in CH_2Cl_2 (3 mL) for 24 h (followed by centrifugation and decantation each time), and was subsequently dried in vacuum for 6 h at RT prior to further investigations to give MFU-2 (15.5 mg, 0.039 mmol, 70% based on H_2-bdpb). IR (KBr): 3432 (br), 3068 (m), 3026 (m), 2926 (m), 1574 (s), 1493 (m), 1427 (s), 1377 (m), 1319 (m), 1285 (m), 1123 (m), 1047 (s), 1013 (s), 984 (w), 847 (m), 789 (w), 677 (w), 614 (w), 581 (m), 487 (m), 437 cm^{-1} (w); elemental analysis calcd (%) for $Co(C_{16}H_{16}N_4) \cdot (C_3H_7NO)$: C 57.6, H 5.9, N 17.7; found: C 57.7, H 5.5, N 17.2.

Microwave-assisted solvothermal synthesis of MFU-2: In a Pyrex sample tube (35 mL), H_2-bdpb (96 mg, 0.40 mmol) and $Co(NO_3)_2 \cdot 6H_2O$ (104 mg, 0.36 mmol) were suspended at RT in DMF (1 mL). The tube was sealed and heated for 8 min at 120 °C by a microwave synthesiser (CEM Discover S) at 300 W, filtered when still hot and washed with hot DMF (3 × 20 mL) and CH_2Cl_2 (10 mL) to obtain phase-pure MFU-2 (142 mg, 0.36 mmol, 90% based on H_2-bdpb).

Catalytic oxidation of cyclohexene by employing *tert*-butyl hydroperoxide: MFU-1 or MFU-2 (0.095 mmol based on cobalt centres) was added to a solution of cyclohexene (16 mmol), *t*BuOOH (8 mmol) and 1,2,4-trichlorobenzene (2 mmol; internal standard) at RT. The reaction mixture was stirred at 70 °C. Aliquots of about 50 μL were removed after time intervals indicated in the main text. Each sample was diluted with CH_2Cl_2 (1 mL) and filtered through a 0.25 μm Acrodisc nylon filter. Then, the sample was analysed by gas chromatography. For investigations on catalyst activities in subsequent multiple runs, the catalysts were separated from the reaction mixture by centrifugation and rinsed twice with CH_2Cl_2 before reuse. To investigate metal leaching from the catalyst, the hot reaction mixture was filtered at the reaction temperature when approximately 50% of the final conversion achieved in a previous run was reached (after 2 h in the case of MFU-1 and after 4.5 h in the case of MFU-2). To investigate the influence of crystal size and catalyst loading on reaction rates, different amounts of MFU-1 from solvothermal or microwave syntheses were reacted as described above. The initial rates were determined at low substrate conversion, after reaction times of 20–40 min. MFU-1 catalyst (0.1 mmol) was reacted with cyclohexene (16 mmol) and *tert*-butyl hydroperoxide (8 mmol). The reaction was filtered hot after 24 h, evaporated to dryness, the residue was dissolved in 0.2% HNO_3 and afterwards analysed by AAS. The solution contained less than 3 μg L^{-1} Co, showing that less than 1.1×10^{-3}% of the catalyst decomposed (for full decomposition of the catalyst, the solution should contain 330 mg L^{-1} of Co). All yields and conversions were based on cyclohexene. Conversions and turnover numbers (TONs) were calculated from the equations: TON = 100% × [sum of products]/[amount of Co], conversion = 100% × [sum of products]/[initial cyclohexene] for catalysis employing *tert*-butyl hydroperoxide (since educt and *tert*-butanol show the same retention times), otherwise conversion = 100% × [consumed educt]/[initial educt].

Catalytic oxidation of hydrocarbons with MFU-1 by employing molecular oxygen: NHPI (0.31 mmol), MFU-1 (0.038 mmol based on cobalt centres) and 1,2,4-trichlorobenzene (1.2 mmol; internal standard) were added to a solution of a hydrocarbon test substrate (3.0 mmol, either cyclohexene (300 μL), ethylbenzene (365 μL), cyclohexanol (270 mg) or cyclohexane (300 μL)) in acetonitrile (5 mL), and the reaction mixture was stirred at 35 °C for 24 h under atmospheric oxygen by using a reflux condenser to avoid the escape of volatile components. Aliquots of about 50 μL were removed after time intervals indicated in the main text. Each sample was diluted with CH_2Cl_2 (1 mL) and filtered through a 0.25 μm Acrodisc nylon filter. Then, the sample was analysed by gas chromatography. To investigate metal leaching from the catalyst, the hot reaction mixture was filtered at a reaction temperature when approximately 50% of the final conversion achieved in a previous run was reached (after 16 h).

For the immobilization of NHPI, MFU-1 (0.038 mmol based on cobalt centres) was suspended for 3 d in a solution of NHPI (0.31 mmol) in acetonitrile (5 mL; same stochiometry as in catalysis reaction). Afterwards, the modified MFU-1 (NHPI@MFU-1) was filtered, washed with acetonitrile and dried in vacuum. The modified catalyst NHPI@MFU-1 was used in the catalysis reaction suspended in cyclohexene (300 μL, 3.0 mmol; as the educt), together with 1,2,4-trichlorobenzene (150 μL, 1.2 mmol; internal standard) and *tert*-butyl hydroperoxide (0.15 mmol; initiator to prevent the otherwise observed initiation time). The mixture was stirred under atmospheric oxygen at 35 °C by using a reflux condenser to avoid the escape of volatile components.

Crystal structure determination of MFU-1 and MFU-2: Intensity data for MFU-1 and MFU-2 were collected at 120 K on a Oxford Diffraction, SuperNova A diffractometer (4-circle kappa goniometer, dual wavelength (Mo,Cu) microfocus X-ray sources, 135 mm CCD detector) using $Mo_{K\alpha}$ radiation ($\lambda = 0.7107$ Å) for MFU-1 and $Cu_{K\alpha}$ radiation ($\lambda = 1.5418$ Å) for MFU-2. Selected crystal, measurement and refinement data are given in Table 1. The data were corrected for Lorentz and polarisation effects and a cylindrical absorption correction[92] was applied for MFU-2. Programs used for data collection: Bruker XSCANS,[93] data reduction: Bruker SHELXTL,[94] structure solution: SHELXS-97,[95] structure refinement: SHELXL-97,[96] molecular graphics: Diamond V3.1.,[97] Mercury V1.5.[98] Structures were solved by using direct methods and refined by full-matrix

least squares on $|F|^2$. Disordered atoms were calculated isotropic in case of non-positive U_{eq}; all others with anisotropic displacement parameters. Hydrogen atoms were placed in geometrically calculated positions. See the Supporting Information for details. CCDC-796315 (MFU-1) and 796314 (MFU-2) contain the supplementary crystallographic data for this paper. These data can be obtained free of charge from The Cambridge Crystallographic Data Centre via www.ccdc.cam.ac.uk/data_request/cif.

DFT calculations: DFT calculations with periodic boundary conditions were carried out by using the gradient corrected Perdew–Burke–Ernzerhofer (PBE)[99] functional employing the VASP[100,101] program package. Dispersion interactions were added semi-empirically[102] following the Grimme[103] scheme. Core electrons were described within the projector augmented wave scheme. An [Ar] core was used for Co, whereas the 4s and 3d electrons were treated explicitly. For C, N and O, the 2s and 2p electrons were treated explicitly. The valence electrons were described by a plane wave basis set with an energy cutoff of 800 eV along with the appropriate PAW potentials. The core radii for Co, O, C, N and H were 2.30, 1.52, 1.50, 1.50 and 1.10 au, respectively.

As a first step, the cell parameters of MFU-1 were computed by applying symmetry restrictions with respect to the T point group. The fractional coordinates were relaxed until the forces were smaller than 0.005 eV Å^{-1}. The MFU-1 was considered to be in the high spin state, that is, 12 unpaired electrons (3 on each Co atom).

For the dioxygen adsorption on MFU-1, calculations on periodic structures were done by using an energy cutoff of 400 eV. In these calculations, the cell parameters were kept constant and only the ionic positions were allowed to relax. The adsorption energies were calculated by $\Delta E = E(O_2\text{–MFU-1}) - E(\text{MFU-1}) - E(O_2)$ and were corrected for thermal contributions at 298 K. The vibrational frequencies were calculated numerically by displacing each ion by a step of 0.015 Å in all three cartesian directions. A more detailed computational study is in preparation.

Details on the crystallographic data, experimental methods and equipment used for investigations are given in the Supporting Information.

Acknowledgements

This work was supported by the German Research Foundation (DFG) within Priority Program 1362. We want to thank BESSY for the granted synchrotron beamtime, especially Prof. Erko at BESSY for fruitful discussions as well as scientific and technical support. Measurement of single-crystal X-ray diffraction data by Oxford Diffraction (now part of Varian), is highly appreciated, in particular, immense support from Dr. Oliver Presly. Dr. Volker Hagen (Rubokat) is acknowledged for his support on the interpretation and evaluation of TPO and isosteric heat of adsorption. We are grateful to Prof. Armando J. L. Pombeiro for suggesting to us the usage of NHPI/PINO. The calculations were carried out at the HLRN supercomputer centre. M.T. is grateful to the Landesgraduiertenförderung Baden-Württemberg for financial support.

[1] For recent reviews on different aspects of MOF applications, see: a) L. J. Murray, M. Dinca, J. R. Long, *Chem. Soc. Rev.* **2009**, *38*, 1294–1314; b) J. R. Li, R. J. Kuppler, H.-C. Zhou, *Chem. Soc. Rev.* **2009**, *38*, 1477–1504; c) A. Corma, H. García, F. X. Llabrés i Xamena, *Chem. Rev.* **2010**, *110*, 4606–4655; d) J. Y. Lee, O. K. Farha, J. Roberts, K. A. Scheidt, S. T. Nguyen, Joseph T. Hupp, *Chem. Soc. Rev.* **2009**, *38*, 1450–1459; e) D. J. Tranchemontagne, J. L. Mendoza-Cortés, M. O'Keeffe, O. M. Yaghi, *Chem. Soc. Rev.* **2009**, *38*, 1257–1283; f) M. Eddaoudi, D. B. Moler, H. Li, B. Chen, T. M. Reineke, M. O'Keeffe, O. M. Yaghi, *Acc. Chem. Res.* **2001**, *34*, 319–330; g) G. Férey, C. Mellot-Draznieks, C. Serre, F. Millange, *Acc. Chem. Res.* **2005**, *38*, 217–225; h) U. Müller, M. Schubert, F. Teich, H. Puetter, K. Schierle-Arndt, J. Pastré, *J. Mater. Chem.* **2006**, *16*, 626–636.

[2] A. U. Czaja, N. Trukhan, U. Müller, *Chem. Soc. Rev.* **2009**, *38*, 1284–1293.

[3] O. M. Yaghi, H. Li, M. Eddaoudi, M. O'Keeffe, *Nature* **1999**, *402*, 276–279.

[4] Y. K. Hwang, D.-Y. Hong, J.-S. Chang, H. Seo, M. Yoon, J. Kim, S. H. Jhung, C. Serre, G. Férey, *Appl. Catal. A* **2009**, *358*, 249–253.

[5] S.-H. Cho, B. Ma, S. T. Nguyen, J. T. Hupp, T. E. Albrecht-Schmitt, *Chem. Commun.* **2006**, 2563–2565.

[6] M. Eddaoudi, J. Kim, N. Rosi, D. Vodak, J. Wachter, M. O'Keefe, O. M. Yaghi, *Science* **2002**, *295*, 469–472.

[7] a) S. Biswas, M. Grzywa, H. P. Nayek, S. Dehnen, I. Senkovska, S. Kaskel, D. Volkmer, *Dalton Trans.* **2009**, 6487–6495; b) M. Dinca, J. R. Long, *J. Am. Chem. Soc.* **2005**, *127*, 9376–9377; c) T. K. Maji, G. Mostafa, H. Ch. Chang, S. Kitagawa, *Chem. Commun.* **2005**, 2436–2438; d) L. Pan, B. Parker, X. Huang, D. H. Olson, J. Y. Lee, J. Li, *J. Am. Chem. Soc.* **2006**, *128*, 4180–4181.

[8] a) F. Stallmach, S. Gröger, V. Künzel, J. Kärger, O. M. Yaghi, M. Hesse, U. Müller, *Angew. Chem.* **2006**, *118*, 2177–2181; b) S. Amirjalayer, M. Tafipolsky, R. Schmid, *Angew. Chem.* **2007**, *119*, 467–470.

[9] S. Hermes, M.-K. Schröter, R. Schmid, L. Khodeir, M. Muhler, A. Tissler, R. W. Fischer, R. A. Fischer, *Angew. Chem.* **2005**, *117*, 6394–6397; *Angew. Chem. Int. Ed.* **2005**, *44*, 6237–6241.

[10] a) M. S. El-Shall, V. Abdelsayed, A. E. R. S. Khder, H. M. A. Hassan, H. M. El-Kaderi, T. E. Reich, *J. Mater. Chem.* **2009**, *19*, 7625–7631; b) M. Sabo, A. Henschel, H. Fröde, E. Klemm, S. Kaskel, *J. Mater. Chem.* **2007**, *17*, 3827–3832.

[11] Y. K. Hwang, D.-Y. Hong, J.-S. Chang, S. H. Jhung, Y.-K. Seo, J. Kim, A. Vimont, M. Daturi, C. Serre, G. Férey, *Angew. Chem.* **2008**, *120*, 4212–4216; *Angew. Chem. Int. Ed.* **2008**, *47*, 4144–4148.

[12] H.-L. Jiang, B. Liu, T. Akita, M. Haruta, H. Sakurai, Q. Xu, *J. Am. Chem. Soc.* **2009**, *131*, 11302–11303.

[13] M. Müller, S. Hermes, K. Kähler, M. W. E. van den Berg, M. Muhler, R. A. Fischer, *Chem. Mater.* **2008**, *20*, 4576–4587.

[14] F. Schröder, S. Henke, X. Zhang, R. A. Fischer, *Eur. J. Inorg. Chem.* **2009**, 3131–3140.

[15] K. S. Suslick, P. Bhyrappa, J.-H. Chou, M. E. Kosal, S. Nakagaki, D. W. Smithenry, S. R. Wilson, *Acc. Chem. Res.* **2005**, *38*, 283–291.

[16] C. D. Wu, A. Hu, L. Zhang, W. Lin, *J. Am. Chem. Soc.* **2005**, *127*, 8940–8941.

[17] a) L. Alaerts, E. Seguin, H. Poelman, F. Thibault-Starzyk, P. A. Jacobs, D. E. De Vos, *Chem. Eur. J.* **2006**, *12*, 7353–7363; b) K. Schlichte, T. Kratzke, S. Kaskel, *Microporous Mesoporous Mater.* **2004**, *73*, 81–88; c) A. Vimont, J. M. Goupil, J. C. Lavalley, M. Daturi, S. Surble, C. Serre, F. Millange, G. Férey, N. Audebrand, *J. Am. Chem. Soc.* **2006**, *128*, 3218–3227; d) P. Horcajada, S. Surble, C. Serre, D. Y. Hong, Y. K. Seo, J. S. Chang, J. M. Greneche, I. Margiolaki, G. Férey, *Chem. Commun.* **2007**, 2820–2822.

[18] B. Xiao, H. Hou, Y. Fan, *J. Organomet. Chem.* **2007**, *692*, 2014–2020.

[19] A. Dhakshinamoorthy, M. Alvaro, H. Garcia, *J. Catal.* **2009**, *267*, 1–4.

[20] F. X. Llabrés i Xamena, O. Casanova, R. G. Tailleur, H. Garcia, A. Corma, *J. Catal.* **2008**, *255*, 220–227.

[21] K. S. Park, Z. Ni, A. P. Cote, J. Y. Choi, R. D. Huang, F. J. Uribe-Romo, H. K. Chae, M. O'Keeffe, O. M. Yaghi, *Proc. Natl. Acad. Sci. USA* **2006**, *103*, 10186–10191.

[22] The van der Waals radius of C (0.17 nm) was used to calculate the width of the apertures: A. Bondi, *J. Phys. Chem.* **1964**, *68*, 441–451.

[23] a) S. A. Moggach, T. D. Bennett, A. K. Cheetham, *Angew. Chem.* **2009**, *121*, 7221–7223; b) G. Férey, C. Serre, *Chem. Soc. Rev.* **2009**, *38*, 1380–1399.

[24] E. L. Wu, G. R. Landolt, A. W. Chester, *Stud. Surf. Sci. Catal.* **1986**, *28*, 547–554.

[25] A. F. Hollemann, E. Wiberg, *Lehrbuch der Anorganischen Chemie, Vol. 101*, de Gruyter, Berlin, **1995**, p. 1220.

[26] H. Irving, R. J. P. Williams, *J. Chem. Soc.* **1953**, 3192–3210.

[27] (μ_4-Oxo)hexakis(μ_2-3,5-dimethylpyrazolato-*N*,*N*′)tetracobalt(II) (CSD ID: LESNUS): M. K. Ehlert, S. J. Rettig, A. Storr, R. C. Thompson, J. Trotter, *Acta Crystallogr. C* **1994**, *50*, 1023–1026.

[28] Catena[bis(μ_2-pyrazolato)cobalt(II)] (CSD-ID: AQOPEB): N. Masciocchi, G. A. Ardizzoia, S. Brenna, G. LaMonica, A. Maspero, S. Galli, A. Sironi, *Inorg. Chem.* **2002**, *41*, 6080–6089.

[29] F. Ramirez, S. B. Bhatia, A. V. Patwardhan, C. P. Smith, *J. Org. Chem.* **1967**, *32*, 3547–3553.

[30] MFU is the acronym for Metal–Organic Framework Ulm University.

[31] M. Tonigold, Y. Lu, B. Bredenkötter, B. Rieger, S. Bahnmüller, J. Hitzbleck, G. Langstein, D. Volkmer, *Angew. Chem.* **2009**, *121*, 7682–7687; *Angew. Chem. Int. Ed.* **2009**, *48*, 7546–7550.

[32] Hexakis(μ_2-acetato-*O*,*O*')(μ_4-oxo)tetrazinc (CSD-ID: ZNOXAC): H. Koyama, Y. Saito, *Bull. Chem. Soc. Jpn.* **1954**, *27*, 112–114.

[33] Similar results were recently reported on the microwave-assisted synthesis of a range of zinc terephthalate based MOFs: Z. Ni, R. I. Masel, *J. Am. Chem. Soc.* **2006**, *128*, 12394–12395.

[34] A. L. Spek, *J. Appl. Crystallogr.* **2003**, *36*, 7–13.

[35] For DMF, a molecular volume of 128 Å^3 was calculated from the molar mass (73.1 g mol^{-1}) and the density at room temperature (0.95 g cm^{-3}). The void volume found by PLATON/SQUEEZE was divided by this value to obtain the approximate number of solvent molecules per elemental cell.

[36] L. Hou, Y.-Y. Lin, X.-M. Chen, *Inorg. Chem.* **2008**, *47*, 1346–1351.

[37] W. Ouellette, A. V. Prosvirin, K. Whitenack, K. R. Dunbar, J. Zubieta, *Angew. Chem.* **2009**, *121*, 2174–2177; *Angew. Chem. Int. Ed.* **2009**, *48*, 2140–2143.

[38] The cobalt(II) ions resemble the tetrahedrally coordinated S atoms in PtS, whereas the organic linker (with its four nitrogen atoms as points of extension) displays a rectangular SBU that resembles the square planar Pt atoms in PtS.

[39] a) Y. Lu, M. Tonigold, B. Bredenkötter, D. Volkmer, J. Hitzbleck, G. Langstein, *Z. Anorg. Allg. Chem.* **2008**, *634*, 2411–2417; b) H. J. Choi, M. Dinca, J. R. Long, *J. Am. Chem. Soc.* **2008**, *130*, 7848–7850.

[40] a) Y. Shimura, R. Tsuchida, *Bull. Chem. Soc. Jap.* **1957**, *30*, 502–505; b) M. Ali, S. K. Saha, P. Banerjee, *J. Chem. Soc. Dalton Trans.* **1991**, 2305–2309.

[41] J. Moellmer, E. B. Celer, R. Luebke, A. J. Cairns, R. Staudt, M. Eddaoudi, M. Thommes, *Microporous Mesoporous Mater.* **2010**, *129*, 345–353.

[42] F. Rouquerol, J. Rouquerol, K. Sing, *Adsorption by Powders and Porous Solids: Principles, Methodology and Applications*, Academic Press, London, **1999**.

[43] S. Ma, H.-C. Zhou, *J. Am. Chem. Soc.* **2006**, *128*, 11734–11735.

[44] a) H. A. Goodwin, *Top. Curr. Chem.* **2004**, *234*, 23–47; b) T. Nowlin, K. Cohn, *Inorg. Chem.* **1972**, *11*, 560–563; c) L. Sacconi, M. Ciampolini, G. P. Speroni, *Inorg. Chem.* **1965**, *4*, 1116–1119; d) M. Ciampolini, N. Nardi, *Inorg. Chem.* **1966**, *5*, 41–44; e) M. J. Norgett, L. M. Venanzi, *Inorg. Chim. Acta* **1968**, *2*, 107–110; f) F. Mani, C. Mealli, *Inorg. Chim. Acta* **1981**, *54*, L77L79.

[45] a) B. L. Vallee, R. J. P. Williams, *Proc. Natl. Acad. Sci. USA* **1968**, *59*, 498–505; b) M. W. G. De Bolster, *Pure Appl. Chem.* **1997**, *69*, 1251–1303.

[46] A. Mavrandonakis, J. Sauer, unpublished results.

[47] S. Ye, F. Neese, *Curr. Opin. Chem. Biol.* **2009**, *13*, 89–98.

[48] a) T. Düren, F. Millange, G. Férey, K. S. Walton, R. Q. Snurr, *J. Phys. Chem. C* **2007**, *111*, 15350–15356; b) K. S. Walton, R. Q. Snurr, *J. Am. Chem. Soc.* **2007**, *129*, 8552–8556.

[49] The error estimate was based on the weighing error.

[50] The reported surface areas for MOF-5 substantially vary in the range 600–3400 m^{2}g^{-1}; see, for example: a) B. Panella, M. Hirscher, *Adv. Mater.* **2005**, *17*, 538–541; b) Y. Li, R. T. Yang, *J. Am. Chem. Soc.* **2006**, *128*, 726–727; c) Y. Li, R. T. Yang, *J. Am. Chem. Soc.* **2006**, *128*, 8136–8137; d) B. Panella, M. Hirscher, H. Pütter, U. Müller, *Adv. Funct. Mater.* **2006**, *16*, 520–524; e) L. Huang, H. Wang, J. Chen, Z. Wang, J. Sun, D. Zhao, Y. Yan, *Microporous Mesoporous Mater.* **2003**, *58*, 105–114.

[51] J. Hafizovic, M. Bjørgen, U. Olsbye, P. D. C. Dietzel, S. Bordiga, C. Prestipino, C. Lamberti, K. P. Lillerud, *J. Am. Chem. Soc.* **2007**, *129*, 3612–3620.

[52] a) A. B. P. Lever, *Inorganic Electronic Spectroscopy*, Elsevier, Amsterdam, **1968**, Chapter 9, p. 323; b) L. Poul, N. Jouini, F. Fiévet, *Chem. Mater.* **2000**, *12*, 3123–3132.

[53] a) K. Nomiya, R. Kobayashi, M. Miwa, *Bull. Chem. Soc. Jpn.* **1983**, *56*, 2272–2275; b) J. H. Ashley, P. C. H. Mitchell, *J. Chem. Soc. A* **1968**, 2821–2827.

[54] D. T. Shay, G. P. A. Yap, L. N. Zakhaov, A. L. Rheingold, K. H. Theopold, *Angew. Chem.* **2005**, *117*, 1532–1534; *Angew. Chem. Int. Ed.* **2005**, *44*, 1508–1510.

[55] R. A. Sheldon, M. Wallau, I. W. C. E. Arends, U. Schuchard, *Acc. Chem. Res.* **1998**, *31*, 485–493.

[56] a) B. Ravel, M. Newville, *J. Synchrotron Radiat.* **2005**, *12*, 537–541; b) M. Newville, *J. Synchrotron Radiat.* **2001**, *8*, 322–324; c) B. Ravel, *J. Synchrotron Radiat.* **2001**, *8*, 314–316; d) J. J. Rehr, R. C. Albers, *Rev. Mod. Phys.* **2000**, *72*, 621–654.

[57] The expected distances for tetrahedral Co ions in the case of Co^{II} are 1.93(6) and 2.00(7) Å for Co–O and Co–N, respectively and in the case of Co^{III} are 1.81(3) and 1.89(5) Å for Co–O and Co–N, respectively. CCDC codes for four-coordinate (tetrahedral) Co^{II}: a) V. Divjakovic, V. Leovac, *Cryst. Struct. Commun.* **1978**, *7*, 689–692 (CSD entry AAMTCO); b) P. E. Kruger, N. Martin, M. Nieuwenhuyzen, *J. Chem. Soc. Dalton Trans.* **2001**, 1966–1970 (CSD entry ABODUQ); c) P. G. Lacroix, F. Averseng, I. Malfant, K. Nakatani, *Inorg. Chim. Acta* **2004**, *357*, 3825–3835 (CSD entry ABUWEA); d) J. Du, L. Han, Y. Cui, J. Li, Y. Li, W.-H. Sun, *Aust. J. Chem.* **2003**, *56*, 703–706 (CSD entry AJEBEW); e) U. Schroder, L. Beyer, R. Richter, J. Angulo-Cornejo, M. Castillo-Montoya, M. Lino-Pacheco, *Inorg. Chim. Acta* **2003**, *353*, 59–67 (CSD entry AJILAG); f) L.-J. Zhang, J.-Q. Xu, Z. Shi, X.-L. Zhao, T.-G. Wang, *J. Solid State Chem.* **2003**, *173*, 32–39 (CSD entry AKAREJ); g) S.-M. Peng, Y.-N. Lin, *Acta Crystallogr. C* **1986**, *42*, 1725–1731 (CSD entry FASHOW); h) F. A. Cotton, L. M. Daniels, L. R. Falvello, J. H. Matonic, C. A. Murillo, X. Wang, H. Zhou, *Inorg. Chim. Acta* **1997**, *266*, 91–102 (CSD entry NEKXAC). Four-coordinate Co^{III}: i) X. Dai, P. Kapoor, T. H. Warren, *J. Am. Chem. Soc.* **2004**, *126*, 4798–4799 (CSD entries ABATIH, ABAVAB); j) C. A. Jimenez, J. B. Belmar, J. Alderete, F. S. Delgado, M. Lopez-Rodriguez, O. Pena, M. Julve, C. Ruiz-Perez, *Dalton Trans.* **2007**, 2135–2144 (CSD entry CIDVIV); k) S. W. Gordon-Wylie, B. L. Claus, C. P. Horwitz, Y. Leychkis, J. M. Workman, A. J. Marzec, G. R. Clark, C. E. F. Rickard, B. J. Conklin, S. Sellers, G. T. Yee, T. J. Collins, *Chem. Eur. J.* **1998**, *4*, 2173–2181 (CSD entry FAJTAL); l) J. Chakraborty, R. K. B. Singh, B. Samanta, C. R. Choudhury, S. K. Dey, P. Talukder, M. J. Borah, S. Mitra, *Z. Naturforsch. B* **2006**, *61*, 1209–1216 (CSD entry VESMEM).

[58] O. Haas, R. P. W. J. Struis, J. M. McBreen, *J. Solid State Chem.* **2004**, *177*, 1000–1010.

[59] a) A. L. Roe, D. J. Schneider, R. J. Mayer, J. W. Pyrz, J. Windom, L. Que, *J. Am. Chem. Soc.* **1984**, *106*, 1676–1678; b) C. R. Randall, L. Shu, Y.-M. Chiou, K. S. Hagen, M. Ito, N. Kitajima, R. J. Lachicotte, Y. Zang, L. Que, *Inorg. Chem.* **1995**, *34*, 1036–1039; c) V. Briois, C. Cartier dit Moulin, M. Momenteau, P. Maillard, J. Zarembowitch, E. Dartyge, A. Fontaine, G. Tourillon, P. Thuéry, M. Verdaguer, *J. Chim. Phys.* **1989**, *86*, 1623–1634.

[60] a) L. Barbey, N. Nguyen, V. Caignaert, F. Studer, B. Raveau, *J. Solid State Chem.* **1994**, *112*, 148.

[61] a) M. Croft, D. Sills, M. Greenblatt, C. Lee, S.-W. Cheong, K. V. Ramanujachary, D. Tran, *Phys. Rev. B* **1997**, *55*, 8726; b) M. C. Sánchez, J. García, J. Blasco, G. Subías, J. Pérez-Cacho, *Phys. Rev. B* **2002**, *65*, 144409; c) M. C. Sánchez, G. Subías, J. García, J. Blasco, *Phys. Rev. B* **2004**, *69*, 184415; d) A. H. de Vries, L. Hozoi, R. Broer, *Int. J. Quantum Chem.* **2003**, *91*, 57.

[62] [Co(pz)$_3$] (pz = pyrazolate) contains Co^{III} ions in an octahedral coordination environment: see ref. [28].

[63] a) C. Giannotti, C. Fontaine, A. Chiaroni, C. Riche, *J. Organomet. Chem.* **1976**, *113*, 57–65; b) A. Nishinaga, H. Tomita, K. Nishizawa, T. Matsuura, S. Ooi, K. Hirotsu, *Chem. Soc. Dalton Trans.* **1981**, 1504–1514; c) L. Saussine, E. Brazi, A. Robine, H. Mimoun, J. Fischer, R. Weiss, *J. Am. Chem. Soc.* **1985**, *107*, 3534–3540; d) F. A.

Chavez, C. V. Nguyen, M. M. Olmstead, P. K. Mascharak, *Inorg. Chem.* **1996**, *35*, 6282–6291.

[64] a) S. Hikichi, H. Komatsuzaki, M. Akita, Y. Moro-oka, *J. Am. Chem. Soc.* **1998**, *120*, 4699–4710; b) S. Hikichi, M. Yoshizawa, Y. Sasakura, H. Komatsuzaki, Y. Moro-oka, M. Akita, *Chem. Eur. J.* **2001**, *7*, 5011–5028; c) O. M. Reinaud, G. P. A. Yap, A. L. Rheingold, K. H. Theopold, *Angew. Chem.* **1995**, *107*, 2171–2173; *Angew. Chem. Int. Ed. Engl.* **1995**, *34*, 2051–2052; d) S. Hikichi, H. Komatsuzaki, N. Kitajima, M. Akita, M. Mukai, T. Kitagawa, Y. Moro-oka, *Inorg. Chem.* **1997**, *36*, 266–267; e) J. W. Egan Jr. , B. S. Haggerty, A. L. Rheingold, S. C. Sendlinger, K. H. Theopold, *J. Am. Chem. Soc.* **1990**, *112*, 2445–2446; f) S. Hikichi, M. Yoshizawa, Y. Sasakura, M. Akita, Y. Moro-oka, *J. Am. Chem. Soc.* **1998**, *120*, 10567–10568; g) C. J. Cramer, W. B. Tolman, K. H. Theopold, A. L. Rheingold, *Proc. Natl. Acad. Sci. USA* **2003**, *100*, 3635–3640.

[65] a) W. J. J. Stevens, V. Meynen, E. Bruijn, O. I. Lebedev, G. Van Tendeloo, P. Cool, E. F. Vansant, *Microporous Mesoporous Mater.* **2008**, *110*, 77–85; b) J. C. Groen, T. Bach, U. Ziese, A. M. Paulaime-van Donk, K. P. de Jong, J. A. Moulijn, J. Pérez-Ramirez, *J. Am. Chem. Soc.* **2005**, *127*, 10792–10793; c) J. C. Groen, S. Abelló, L. A. Villaescusa, J. Pérez-Ramirez, *Microporous Mesoporous Mater.* **2008**, *114*, 93–102; d) J. C. Groen, J. A. Moulijn, J. Pérez-Ramirez, *J. Mater. Chem.* **2006**, *16*, 2121–2131; e) J. C. Groen, J. A. Moulijn, J. Pérez-Ramirez, *J. Ind. Eng. Chem. Res.* **2007**, *46*, 4193–4201.

[66] a) F. A. Chavez, J. M. Rowland, M. M. Olmstead, P. K. Mascharak, *J. Am. Chem. Soc.* **1998**, *120*, 9015–9027; b) F. A. Chavez, J. A. Briones, M. M. Olmstead, P. K. Mascharak, *Inorg. Chem.* **1999**, *38*, 1603–1608; c) R. A. Sheldon, J. K. Kochi, *Metal-Catalyzed Oxidations of Organic Compounds*, Academic Press, New York, **1981**; d) A. Bravo, H.-R. Bjørsvik, F. Fontana, L. Liguori, F. Minesci, *J. Org. Chem.* **1997**, *62*, 3849–3857; e) S. J. Blanksby, G. B. Ellison, *Acc. Chem. Res.* **2003**, *36*, 255–263; f) S. P. Heneghan, S. W. Benson, *Int. J. Chem. Kinet.* **1983**, *15*, 815–822.

[67] a) T. R. Rizzo, B. D. Cannon, E. S. McGinley, F. F. Crim, *Laser Chem.* **1983**, *2*, 321–333; b) A. C. Baldwin in *The Chemistry of Functional Groups, Peroxides* (Ed.: S. Patai), Wiley, New York, **1983**, p. 279; c) G. Dayma, P. A. Glaude, R. Fournet, F. Battin-Leclerc, *Int. J. Chem. Kinet.* **2003**, *35*, 273–285; d) D. de B. Darwent, *Bond Dissociation Energies in Simple Molecules*, NBSDS-NBS, 31, GPO, Washington, DC, **1970**.

[68] Measured at 298 K in benzene: D. V. Avila, K. U. Ingold, J. Lusztyk, W. A. Green, D. R. Procopio, *J. Am. Chem. Soc.* **1995**, *117*, 2929–2930.

[69] a) M. V. Encina, M. Rivera, E. A. Lissi, *J. Polym. Sci. Polym. Chem. Ed.* **1978**, *16*, 1709–1717; b) H. Paul, R. D. Small, J. C. Scaiano, *J. Am. Chem. Soc.* **1978**, *100*, 4520–4527; c) M. V. Encinas, J. C. Scaiano, *J. Am. Chem. Soc.* **1981**, *103*, 6393–6397; d) J. H. B. Chenier, S. B. Tong, J. A. Howard, *Can. J. Chem.* **1978**, *56*, 3047–3053.

[70] S. E. Bottle, W. K. Busfield, I. D. Jenkins, *J. Chem. Soc. Perkin Trans. 2* **1992**, 2145–2150.

[71] W. K. Busfield, I. D. Grice, I. D. Jenkins, S. H. Tang, *Aust. J. Chem.* **1991**, *44*, 1407–1415.

[72] T. W. Campbell, G. M. Coppinger, *J. Am. Chem. Soc.* **1951**, *73*, 1788–1789.

[73] a) I. W. C. E. Arends, K. U. Ingold, D. D. M. Wayner, *J. Am. Chem. Soc.* **1995**, *117*, 4710–4711; b) H. Fischer, *J. Am. Chem. Soc.* **1986**, *108*, 3925–3927; c) B. E. Daikh, R. G. Finke, *J. Am. Chem. Soc.* **1992**, *114*, 2938–2943.

[74] L. Salem, *Electrons in Chemical Reactions: First Principles*, Wiley, New York, **1982**.

[75] G. Henrici-Olivé, S. Olivé, *Angew. Chem.* **1974**, *86*, 1–12; *Angew. Chem. Int. Ed. Engl.* **1974**, *13*, 29–38.

[76] No reaction was observed between molecular oxygen and ethene, propene or CO as educts in gas-phase reactions in the presence of MFU-1 at different reaction conditions (1–6 bar, flow rate 4–20 mL min^{-1}, 90–200 °C). An exothermic reaction was observed at 200 °C only in the case of CO, which, according to XRD measurements, was due to the formation of Co_3O_4. The liquid-phase oxidation of cyclohexene did not show a measurable conversion after 72 h at 4 bar oxygen pressure at 50 °C in the presence of MFU-1.

[77] J. Piera, J.-E. Bäckvall, *Angew. Chem.* **2008**, *120*, 3558–3576; *Angew. Chem. Int. Ed.* **2008**, *47*, 3506–3523.

[78] a) Y. Ishii, S. Sakaguchi, T. Iwahama, *J. Org. Chem.* **1996**, *61*, 4520–4526; b) Y. Yoshino, Y. Hayashi, T. Iwahama, S. Sakaguchi, Y. Ishii, *J. Org. Chem.* **1997**, *62*, 6810–6813.

[79] E. Lemaire, A. Rassat, *Tetrahedron Lett.* **1964**, *5*, 2245–2248.

[80] R. Amorati, M. Lucarini, V. Mugnaini, G. F. Peduli, F. Minisci, F. Recupero, F. Fontana, P. Astolfi, L. Greci, *J. Org. Chem.* **2003**, *68*, 1747–1754.

[81] a) S. Coseri, *Catal. Rev.* **2009**, *51*, 218–292; b) F. Recupero, C. Punta, *Chem. Rev.* **2007**, *107*, 3800–3842; c) Y. Ishii, s. Sakaguchi, T. Iwahama, *Adv. Synth. Catal.* **2001**, *343*, 393–427.

[82] L. Horner, W. Jurgleit, *Justus Liebigs Ann. Chem.* **1955**, *591*, 138–152.

[83] a) V. P. Kurkov, J. Z. Pasky, J. B. Lavigne, *J. Am. Chem. Soc.* **1968**, *90*, 4743–4744; b) R. A. Budnik, J. K. Kochi, *J. Org. Chem.* **1976**, *41*, 1384–1389.

[84] F. Rajabi, J. H. Clark, B. Karimi, D. J. Macquarrie, *Org. Biomol. Chem.* **2005**, *3*, 725–726.

[85] Reaction conditions: cyclohexene (300 μL), 1,2,4-trichlorobenzene (150 μL, 1.2 mmol; internal standard), MFU-1 (15 mg), *tert*-butyl hydroperoxide (15 μL, 1 mol %; initiator), atmospheric oxygen, T = 35 °C.

[86] G. W. Parshall, S. D. Ittel in *Homogenous Catalysis: The Applications and Chemistry of Catalysis by Soluble Transition Metal Complexes*, 2nd ed., Wiley, New York, **1992**, pp. 255–261.

[87] M. A. Warpehoski, B. Chabaud, K. B. Sharpless, *J. Org. Chem.* **1982**, *47*, 2897–2900.

[88] a) A. Erko, I. Packe, C. Hellwig, M. Fieber-Erdmann, O. Pawlitzki, M. Veldkamp, W. Gudat, *AIP Conf. Proc.* **2000**, *521*, 415–418; b) A. Erko, I. Packe, W. Gudat, N. Abrosimov, A. Firsov, *SPIE* **2001**, *4145*, 122–128.

[89] F. Dreisbach, H. W. Lösch, *J. Therm. Anal. Calorim.* **2000**, *62*, 515–521.

[90] J. U. Keller, R. Staudt, *Gas Adsorption Equilibria: Experimental Methods and Adsorption Isotherms*, Springer, New York, **2004**.

[91] a) R. Span, W. Wagner, *Int. J. Thermophys.* **2003**, *24*, 1–39; b) R . Span, W. Wagner, *Int. J. Thermophys.* **2003**, *24*, 41–109; c) R. Span, W. Wagner, *Int. J. Thermophys.* **2003**, *24*, 111–162.

[92] C. W. Dwiggins, Jr., *Acta Crystallogr. A* **1975**, *31*, 146–148.

[93] Bruker, XSCANS, Version 2.2, Bruker Analytical X-ray Systems, Madison, WI, **1996**.

[94] SHELXTL V6.12 2000, Bruker Analytical X-Ray Systems, Madison, WI.

[95] G. M. Sheldrick, *Acta Crystallogr. A* **1990**, *46*, 467–473.

[96] G. M. Sheldrick, SHELXL-97, Program for X-ray Crystal Structure Refinement, University of Göttingen, Göttingen (Germany), **1997**.

[97] Diamond–Crystal and Molecular Structure Visualization, Crystal Impact, K. Brandenburg & H. Putz GbR, Bonn (Germany).

[98] Mercury: visualization and analysis of crystal structures, C. F. Macrae, P. R. Edgington, P. McCabe, E. Pidcock, G. P. Shields, R. Taylor, M. Towler, J. van de Streek, *J. Appl. Crystallogr.* **2006**, *39*, 453–457.

[99] J. P. Perdew, K. Burke, M. Ernzerhof, *Phys. Rev. Lett.* **1996**, *77*, 3865.

[100] G. Kresse, J. Furthmüller, *Comput. Mater. Sci.* **1996**, *6*, 15–50.

[101] G. Kresse, J. Furthmuller, *Phys. Rev. B* **1996**, *54*, 11169–11186.

[102] T. Kerber, M. Sierka, J. Sauer, *J. Comput. Chem.* **2008**, *29*, 2088–2097.

[103] S. Grimme, *J. Comput. Chem.* **2006**, *27*, 1787–1799.